Open access • Journal Article • DOI:10.1146/ANNUREV-PHYSCHEM-032511-143716

DEER distance measurements on proteins — **Source link** ⧉

Gunnar Jeschke

Institutions: ETH Zurich

Related papers:

- DeerAnalysis2006 - a comprehensive software package for analyzing pulsed ELDOR data

- Dead-time free measurement of dipole-dipole interactions between electron spins.

- Long-range distance determinations in biomacromolecules by EPR spectroscopy.

- Distance measurements on spin-labelled biomacromolecules by pulsed electron paramagnetic resonance

- Rotamer libraries of spin labelled cysteines for protein studies

DEER Distance Measurements on Proteins

Review Article

Author(s):
Jeschke, Gunnar

Publication date:
2012-05

Permanent link:
https://doi.org/10.3929/ethz-a-010784314

Rights / license:
In Copyright - Non-Commercial Use Permitted

Originally published in:
Annual Review of Physical Chemistry 63, https://doi.org/10.1146/annurev-physchem-032511-143716

DEER Distance Measurements on Proteins

Gunnar Jeschke

Laboratory of Physical Chemistry, ETH Zürich, 8093 Zürich, Switzerland;

email: gjeschke@ethz.ch

Key Words　electron paramagnetic resonance (EPR), electron electron double resonance (ELDOR), spin labeling, structure determination, macromolecular movements, membrane proteins

Abstract　Distance distributions between paramagnetic centers in the range from 1.8 to 6 nm in membrane proteins and up to 10 nm in deuterated soluble proteins can be measured by the DEER technique. The number of paramagnetic centers and their relative orientation can be characterized. DEER does not require crystallization and is not limited with respect to the size of the protein or protein complex. Diamagnetic proteins are accessible by site-directed spin labeling. To characterize structure or structural changes, the experimental protocols were optimized and techniques for artifact suppression were introduced. Data analysis programs were developed and it was realized that interpretation of the distance distributions must take into account the conformational distribution of spin labels. First methods have appeared for deriving structural models from a small number of distance constraints. The current scope and limitations of the technique are illustrated.

CONTENTS

1   Introduction

The double electron electron resonance (DEER) technique, alternatively called
pulsed electron double resonance (PELDOR), separates pairwise couplings be-
tween electron spins from other electron spin interactions. The interactions are
observed in time domain by an approach reminiscent of the spin-echo double res-
onance (SEDOR) experiment used in NMR (1). Decay of the time domain signal
due to transverse electron spin relaxation is factored out by applying an observer
echo sequence of constant duration. This approach, introduced by Milov *et al.*
(2,3) was later extended to a four-pulse sequence for measuring the signal without
dead time on standard commercial pulse electron parmagnetic resonance (EPR)
spectrometers (4, 5). The resulting four-pulse DEER experiment has become
the most widely used approach for measuring distances between electron spins
in biomacromolecules in the range between about 1.8 and 6 nm, in exceptional
cases up to 8 nm (6–8).

Early applications of DEER to pairs of cofactors in photosynthetic reaction
centers were summarized in 1998 (9). Several developments around the turn of
the millenium transformed DEER from a niche application to a tool that com-
plements x-ray crystallography, NMR spectroscopy, and electron microscopy in
biostructural work. First, the potential of site-directed spin labeling (SDSL)

(10) for characterization of proteins without native paramagnetic centers had been fully understood by the year 2000 (11). Second, two new experiments for dead-time free measurements, double-quantum EPR (DQ-EPR) (12) and four-pulse DEER (5) were introduced, which spurred competition. The latter experiment could be adopted by laboratories without previous experience in pulse EPR method development. Third, these techniques could provide not only a single number for the distance, but the distance distribution (13). Thus, characterization of conformational distributions in proteins on a nanometer length scale became feasible.

Around the same time a number of early applications demonstrated the feasibility of DEER and double-quantum EPR studies on spin-labeled peptides (14), soluble proteins (15, 16), a pair of tyrosyl radicals in ribonucleotide reductase (RNR) (17), and integral membrane proteins (18). For the N-terminal domain of major plant light harvesting complex II (LHCII), which was missing in crystal structures, information on the conformational distribution could be obtained (19).

Early development of the technique (20), the underlying physics and relation to distance measurements by solid-state NMR (21), the relation to other EPR techniques for distance measurements (7), and optimization of experimental conditions as well as data analysis (6) have been reviewed before. The present review provides an overview of methodological issues in DEER studies of protein structure and function. Selective application examples focus on typical strategies of DEER studies and on intricacies of data interpretation.

For didactical reasons, the review does not follow the same sequence of steps as a DEER study on proteins. Such a study starts with definition of the bi-

ological question to be answered and proceeds with a selection of the type of paramagnetic centers (Section 2.4) and, if applicable, labeling sites (Section 5.2). Then a mutant plasmid is prepared, protein is produced and labeled, and activity or structure of the modified protein is verified. For membrane proteins the reconstitution procedure may have to be validated and optimized. Then DEER measurements are performed with the proper measurement protocols and under optimized conditions (Section 2.1-2.2). Data are analyzed in terms of distances, distance distributions, number of coupled spins, or angle constraints (Section 4). Interpretation requires at least implicit modeling of the structure or a structural change from sparse distance constraints (Section 5.2). Results of each step need to be validated, key data need to be reproduced, and control measurements on supposedly unlabeled and singly labeled mutants must be performed at least once for each new protein. This review explains intricacies of these steps, so that readers can avoid mistakes that may invalidate a whole elaborate study.

2 Experimental aspects

2.1 Pulse sequence

The four-pulse DEER sequence (5) consists of a refocused primary echo sequence at the observer frequency ω_A with fixed interpulse delays and an inversion pulse at the pump frequency ω_B, which is applied at a variable time t with respect to the first observer echo (Figure 1a). The observer sequence refocuses inhomogeneous broadening of the EPR line of the observer spin A (blue), including g value dispersion, hyperfine couplings, and the coupling of the spin A to those electron spins that are not excited by the observer pulses. Transverse relaxation of spin A and couplings to other electron spins that are excited by the observer pulses

lead to echo attenuation by a factor $\exp\left[-2k(\tau_1 + \tau_2)\right]$. The decay rate constant $k = 1/T_{2,\mathrm{A}} + k_{\mathrm{ID}}$ depends on transverse relaxation time $T_{2,\mathrm{A}}$ of the A spins and on the instantaneous diffusion rate $k_{\mathrm{ID}} = c_{\mathrm{A}} K_{\mathrm{A}}$, which is proportional to the concentration c_{A} of A spins. Signal loss thus increases with increasing interpulse delays τ_1 and τ_2 and increasing concentration c_{A}. The instantaneous diffusion strength K_{A} is inversely proportional to the length of the observer π pulses and has an approximate value of $0.25~\mathrm{mM}^{-1}~\mu\mathrm{s}^{-1}$ for nitroxide spin labels at X-band frequencies (≈ 9.6 GHz) with 32 ns observer π pulse length.

Of the electron spins B that are coupled to observer spin A, a fraction $\lambda < 1$ is excited by the pump pulse at frequency ω_{B} that inverts the state of these spins (red), see Figure 1*b*. With a 12 ns pump pulse at X-band frequency (≈ 9.6 GHz) the inversion efficiency for nitroxide labels is $\lambda \approx 0.5$; it depends slightly on resonator bandwidth and linewidth in the nitroxide EPR spectrum. Inversion of spin B_i changes frequency of spin A by the electron-electron coupling $\omega_{ee,i}$ (Figure 1c), which leads to a phase gain $\phi_i = \omega_{ee,i} t$ of a fraction λ_i of the A spin magnetization. As a consequence the echo amplitude as a function of time t is given by

$$v\left(t\right) = \prod_i \left\{1 - \lambda_i \left[1 - \cos\left(\omega_{ee,i} t\right)\right]\right\} ,\tag{1}$$

where the product runs over all spins B_i coupled to spin A.

If and only if both pump and observer excitation bandwidths are much larger than the electron-electron coupling, the factors λ_i in Eq. (1) are independent of electron-electron coupling (22). Observer echo phase differs in the presence and absence of the pump pulse due to a Bloch-Siegert shift of the A spins induced by the pump pulse (23), which is corrected for by receiver phase adjustment.

Application of DEER as a technique for measuring distance distributions de-

pends on the following additional assumptions, which will be discussed in more detail below. First, exchange coupling between the electron spins is neglected and both spins are assumed to be quantized along the external magnetic field. Thus, the coupling simplifies to the magnetic dipole-dipole coupling $\omega_{ee,i} = (C_i/r_i^3)\left(1 - 3\cos^2\theta_i\right)$, where C_i is proportional to the product of the g values of the A and B spin and takes a value of 52.2 MHz nm^{-3} for $g_A = g_B = 2.0055$ (isotropic g value of nitroxide labels). Here θ_i is the angle between the spin-spin vector and the external magnetic field (Figure 2d). Second, a semi-isolated spin pair is assumed, i.e. for a given observer spin A only one spin B in the same protein molecule or complex is assumed to be within the sensitive distance range of DEER. All B$_i$ spins in other molecules can be considered as homogeneously distributed in space. The assumption of homogeneous spatial distribution can be relaxed to a homogeneous distribution with fractional dimension D (24), for instance $D \approx 2$ for membrane proteins in liposomes. Third, the correlation between λ_i and $\omega_{ee,i}$, which arises from dependence of both quantities on θ_i, is neglected, and an orientation average is taken. With these assumptions, Eq. (1) converts to an expression for a macroscopically disordered sample

$$V\left(t\right) = \left\{1 - \lambda\left[1 - \int_0^1 \cos\left(\frac{C_i}{r_i^3}\left(1 - 3\cos^2\theta_i\right)t\right)\mathrm{d}\cos\theta\right]\right\}B\left(t\right), \qquad (2)$$

where the background function takes the form $B\left(t\right) = \exp\left(-c_B K_B t^{D/3}\right)$. If more than one B spin within the molecule is within the sensitive distance range, the signal takes the form $V(t) = F(t)B(t)$ with the form factor $F(t)$ being the product of all possible pair contributions (25).

The simple factorization of the multi-spin signal expressed by Eq. (1) into an analytically known intermolecular background factor $B(t)$ and intramolecular form factor $F(t)$ sets DEER apart from single-frequency techniques for distance

measurements, such as double-quantum EPR (12) or SIFTER (26). It has been wrongly claimed that the larger modulation depth of DQ-EPR makes background correction less important (27). In fact, the signal of a semi-isolated spin pair in DQ-EPR or SIFTER formally still is a product of the pair form factor $F(t)$ and a background function $B(t)$, only the form of $B(t)$ is not analytically known and strongly depends on the excitation profile of the pulses and EPR lineshape. This complicates extraction of a reliable form factor $F(t)$ and thus of the width and shape of distance distributions.

The constant-time approach of the original DEER experiment entails a sensitivity loss with respect to a variable-time version (28). However, in situations where instantaneous diffusion is significant and spatial distribution of spins is not homogeneous in three dimensions, variable-time DEER fails to exactly compensate for transverse relaxation. Such situations are commonly encountered for membrane proteins reconstituted into liposomes. Taken together these considerations suggest that four-pulse DEER (5) is the method of choice for distance distribution measurements on proteins in most situations.

2.2   Sensitivity

2.2.1   CONCENTRATION   We have extended our previous approach for deriving an optimum concentration (6) by considering the reduction in signal-to-noise ratio of $F(t)$ due to dampening by $B(t)$. With the labeling efficiency f (ratio of the number of B spins to the number of possible B spin sites in the protein) and the maximum dipolar evolution time $t_{\max}$ (Figure 1a), the optimum concentration [mM] for standard X-band DEER with an observer π pulse length of 32 ns and a pump pulse length of 12 ns is $1.38/(f t_{\max})$, if $t_{\max}$ is inserted in μs .

Usually protein expense limits concentration to lower values than that. For the longest $t_{\max}$ of 25 μs achieved to date for a protein (29) and complete labeling ($f = 1$) the optimum concentration is approximately 50 μM. This assumes that local concentration of B spins in the vicinity of A spins equals bulk concentration, which does not apply to membrane proteins in liposomes (30). Depending on the extent of protein crowding in the bilayer, the optimum concentration can be significantly lower than predicted by the formula.

2.2.2 TEMPERATURE AND DEUTERATION   The length of the four-pulse DEER sequence exceeds $2t_{\max}$ by $2(\tau_1 + t_{\mathrm{s}})$, where t_{s} is the minimum spacing between the pump and last observer pulse for which end artifacts in the signal are avoided (Figure 1a). The required $t_{\max}$ depends on the distance to be measured (6) and is typically of the order of $T_{2,\mathrm{A}}$ or even longer. As signal intensity decays exponentially with $1/T_{2,\mathrm{A}}$, sensitivity increases strongly with prolongation of $T_{2,\mathrm{A}}$. Therefore, DEER experiments are best performed in the low temperature limit of transverse relaxation, which is typically reached in proteins labeled with nitroxides at temperatures between 40 and 60 K (6). In this limit transverse relaxation of electron spins is driven by proton spin diffusion, so that deuteration of the matrix improves sensitivity or allows to increase $t_{\max}$ and thus measure longer distances. Often only the buffer and cryoprotectant are deuterated (28). However, protein deuteration further prolongates $T_{2,\mathrm{A}}$ (29), which can extend DEER distance range for soluble proteins to 10 nm or even beyond.

2.2.3 RECONSTITUTION CONDITIONS   When reconstituted in liposomes rather than solubilized in detergent micelles, membrane proteins generally exhibit shorter apparent transverse relaxation times. At bulk concentrations used for DEER, this effect arises from confinement of the spin-labeled protein to the liposome

walls, which enhances local spin concentration. This effect can only partially be compensated by increasing the lipid-to-protein ratio and may be aggravated by the tendency of membrane proteins to distribute unevenly in lipid bilayers (30). Effects of enhanced local concentration were addressed in a model study (31).

These considerations seem to call for a Scylla and Charybdis choice between enhanced local spin concentration in liposomes or the less physiological environment in detergent micelles, the latter being known to alter structural dynamics. Reconstitution into nanodiscs (32) or other nanoassemblies (33) may avoid both disadvantages, albeit at the cost of more expensive and harder reconstitution conditions.

2.2.4 MICROWAVE FREQUENCY BAND   Although to date most DEER experiments on proteins have been performed at X-band frequencies, it was recognized early that signal-to-noise improves at Q-band frequencies of about 34 GHz (34). The huge sensitivity increase at modest microwave (MW) power claimed in later work (35) cannot be reproduced in our hands and is most likely a result of not fully optimizing the X-band measurement. More realistic results were reported later (33, 36), although the X-band data taken for comparison still suffer from three times longer pump pulses than would have been been possible with available MW power. On the other hand, Q-band DEER sensitivity at given concentration can be further enhanced by using a high-power setup and a probehead that allows for oversized samples (37). For organic radical cofactors DEER sensitivity with moderate MW power may decrease at Q-band due to dominance of electron Zeeman broadening (38).

Further frequency increase to W band (94 GHz) still allows for a decrease in sample volume and thus an increase in absolute sensitivity, whereas signal-to-

noise ratio at given concentration decreases. This sensitivity loss is due to a less favorable ratio between excitation bandwidth and spectral width, which in turn leads to dramatic loss in B spin inversion efficiency λ (39). The problem can be overcome by supplying large MW power, thus allowing W-band DEER to be measured down to concentrations of 1 μM (40). Further frequency increase is not expected to offer a sensitivity advantage, but is of interest for determining relative orientations of radical cofactors. Sufficient sensitivity for measurements at effective spin pair concentrations of about 250 μM has been demonstrated at 180 GHz (41).

2.3   Avoiding artifacts

2.3.1   ORIENTATION SELECTION   Data analysis in terms of distance distributions neglects correlation between B spin inversion efficiency λ_i and electron-electron coupling $\omega_{ee,i}$ by assuming that values of angle θ_i (Figure 2d) are selected with probability $\sin\theta_i$, corresponding to an isotropic powder average. Since both pump and observer pulses are selective, this assumption does not apply if the spectra of A and B spins are broadened by anisotropic interactions (Figure 2a,b) and the orientations of the molecular frames of A and B spins are strongly correlated (42). The latter situation is common for paramagnetic cofactors, but rare for nitroxide spin labels, which tend to exhibit broad conformational distributions. If the pump frequency is set to the maximum of the nitroxide spectrum at X or Q band, $\lambda_i \approx 0.3\ldots0.5$ is achieved and orientation selection by the pump pulse can be neglected. The form factor is then almost invariably dominated by the dipolar frequency at $\theta_i = 90°$, which allows for correct determination of the mean distance. Part of the distortions in the distance distribution due to

missing orientations near to $\theta_i = 0°$ (Figures 2e,f, 3d) can be suppressed by a non-negativity constraint for the distance distribution $P(r)$ (Figure 3f). Accordingly, effects of orientation selection may be surprisingly weak for spin-labeled proteins even at W-band frequencies (39).

Strong suppression of orientation selection can be achieved by adding DEER traces obtained with the same pump and observer frequencies at different magnetic fields (Figure 2b) (43). This procedure measures most traces under non-optimum conditions and thus entails some sensitivity loss. Orientation selection is not completely canceled by such field averaging (44). Averaging over different settings of pump and observer frequency was also proposed (45), but requires repetition of pulse channel setup for each new setting, whereas field averaging can be automated as a two-dimensional experiment.

2.3.2   NUCLEAR MODULATION ARTIFACTS   Under conditions that provide optimum sensitivity, excitation bands of the pump and observer pulses slightly overlap. Hence, there is a small probability for excitation of forbidden electron-nuclear transitions of A spins by the pump pulse, which leads to nuclear modulation in the DEER signal (5). The most prominent modulation arises from matrix protons or deuterons. Proton modulation at about 14 MHz at X-band frequencies corresponds to distances around 1.55 nm that are shorter than the lower distance limit of DEER. If such oscillations are strong, they may cause uncertainty in separation of the primary dipolar evolution data into $F(t)$ and $B(t)$. Deuterium modulation at about 2 MHz correspond to distances around 3 nm and thus causes artifacts (Figure 3g). At Q-band frequencies, the deuterium modulations at about 8 MHz cause artifacts at about 2 nm.

Nuclear modulation artifacts can be strongly suppressed by systematic varia-

tion of interpulse delay τ_1 (26,28). For protonated matrices at X-band frequencies adding traces for eight values of τ_1 with increments $\Delta\tau_1 = 8$ ns provides good results. For deuterated matrices, eight values with $\Delta\tau_1 = 56$ ns are appropriate. At Q-band frequencies proton modulations are less prominent, whereas deuterium modulations can be suppressed with $\Delta\tau_1 = 16$ ns.

2.3.3   OVERLAP OF OBSERVER AND PUMP EXCITATION BANDS   Due to overlap of the excitation bands of the pump and observer pulses a small fraction of A spins undergoes the spin dynamics as in the 2+1 train experiment (46). Dipolar modulation in this experiment is not described by Eq. (2). Most notably a growing dipolar oscillation is introduced near $t_{\max}$ where the pump pulse approaches the final refocusing pulse. At the cost of sensitivity this end artifact can be suppressed by decreasing excitation bandwidths, by increasing the frequency difference between pump and observer pulses, or by increasing the difference between τ_2 and $t_{\max}$. For standard X-band conditions (32 ns observer pulses, 12 ns pump pulse, 65 MHz frequency difference), the end artifact is usually negligible.

2.3.4   COMBINATION FREQUENCIES FOR MULTIPLE SPINS   If more than two paramagnetic centers are situated in a protein or protein complex, the pump pulse may excite more than one spin B_i near a given A spin. The form factor $F(t)$ then contains products of the pair form factors $f_i(t)$ for the individual A-B_i spin pairs (25). Thus, products of cosine functions of the dipolar frequencies $\omega_{ee,i}$ occur, which correspond to sum and difference combinations of these frequencies. The relative contribution of combination frequencies scales with $f\lambda$ and these frequencies cause artifacts in the distance distribution at shorter and longer distances than are really present.

These artifacts can be eliminated by systematic variation of λ (25) or sup-

pressed by decreasing λ, for instance by decreasing pump pulse power. If a model of the protein structure is known, the software MMM (47) allows to simulate the effect of combination frequencies on $F(t)$. Work on a general, software-based correction procedure is in progress.

2.3.5   INFLUENCE OF EXCHANGE COUPLING AND VALIDITY OF THE POINT-DIPOLE APPROXIMATION   At distances longer than 1.5 nm, through-space exchange coupling is much smaller than dipole-dipole coupling (48) and thus does not introduce artifacts in the distance distribution. Through-bond exchange coupling is negligible if conjugation between the paramagnetic centers is broken, as is the case for all spin labels used to date in proteins. This is also a good approximation for radical cofactors at distances accessible by DEER. Exchange couplings are detectable by DEER if two radicals are connected by a fully conjugated pathway (49, 50).

A theoretical study addressed the distance error introduced by using the point-dipole approximation with the assumption that the unpaired electron is localized in the midpoint of the N-O bond of a nitroxide (50). According to computations for the relevant saturated-linker case, dipole-dipole coupling is underestimated by the point-dipole approximation by 35% at 1.75 nm and 20% at 2.0 nm. Hence, for a real 1.75 nm distance one would expect to measure an apparent 1.52 nm distance and for a 2.00 nm distance a 1.86 nm distance. These predictions are at odds with experimental studies on model compounds with N-O midpoint distances of about 2 nm (5, 42, 48, 49), which found much better agreement. Assuming an N-O bond length of 0.13 nm, 45% of the spin density being localized at the nitrogen and 50% on the oxygen atom and the remaining 5% being 0.25 nm closer to the partner spin than the N-O midpoint, we have computed the maximum

expected distance error as a function of distance. We find that the true distance is underestimated by less than 0.04 nm for distances larger than 1.5 nm and by less than 0.03 nm for distances larger than 2.5 nm. This result is in agreement with experimental findings and implies that errors due to the point-dipole approximation are negligible compared to uncertainty of spin label conformation. The analogous argument does not necessarily apply to cofactor radicals, which often have much broader spatial distribution of the electron spin and very rigidly defined geometry.

2.4 Types of paramagnetic centers

Most DEER studies on proteins apply SDSL techniques and the overwhelming majority uses the methanethiosulfonate spin label (MTSL) (51), which attaches to genetically engineered cysteine residues. Advantages of MTSL are high selectivity to thiol groups and a good compromise between rigidity and flexibility, ensuring minimal perturbation of protein structure combined with tolerable spatial distribution of the N-O group. The disadvantage is attachment by a disulfide bond, which is prone to reductive cleavage. In the reductive milieu inside living cells (52) or in the presence of cofactors that require slightly reducing conditions (53), maleimido- (MSL) or iodoacetamido-spin labels (IASL) can be used. Five-membered ring nitroxides are more stable under reducing conditions or at low pH values than six-membered ones (54).

As an alternative to cysteine engineering the unnatural amino acid p-acetyl-L-phenylalanine can be genetically encoded and labeled with a hydroxylamine spin label (55). The resulting larger and more flexible side group causes a broader spatial distribution of the N-O position, yet this strategy is very attractive for

proteins with functionally important cysteine residues.

The (2,2,6,6-tetramethyl-piperidine-1-oxyl-4-amino-4-carboxylic acid) spin label TOAC (56) is an artificial amino acid that can be introduced by solid-state (57) or solution (58) peptide synthesis. Spiro linkage of the six-membered nitroxide to the C^α atom causes a very narrow spatial distribution of the N-O group. Since TOAC is a helicogenic amino acid and the sidegroup is virtually unflexible, labeling sites must be judiciously selected. A bulkier analogon of TOAC with the methyl groups being replaced by spiro-cyclohexyl groups reaches the low-temperature limit of transverse relaxation already at about 100 K (59).

Isotope labeling by ^{15}N or deuterium can be used to disentangle distance distributions (60). Such a strategy requires an orthogonal labeling approach, where different labels can be introduced at preselected sites. Orthogonal labeling is simple for self-assembling protein complexes if the components can be expressed, purified, and labeled separately.

Application of DEER to organic radical cofactors is similar to the case of nitroxide spin labels, whereas pump and observer positions and excitation bandwidths need to be optimized for each particular case. Distances can also be measured between metal centres, provided that the ratio of pump pulse excitation bandwidth and EPR spectral width allows for sufficient inversion efficiency λ. This situation is encountered for Cu^{2+}-Cu^{2+} pairs (61). When both pump and observer pulses were applied near the maximum of the EPR spectrum, orientation selection was tolerable and measured distances were in good agreement with the ones found in crystal structures (62). However, later work on a doubly labeled peptide indicated that full analysis of the orientation selection may be required for Cu^{2+}-Cu^{2+} pairs (63).

DEER measurements on Gd^{3+}-Gd^{3+} pairs with spin quantum number $S = 7/2$ of the individual centers appear even more attractive (65). The Gd^{3+} centers can be introduced as labels. High-quality DEER data were obtained with about 3 μL of 60 μM solution at W-band frequency on p75 neurotrophin receptor and the C-terminal domain of the τ subunit of a DNA polymerase (66). Results with chelate ligands, which enclose Gd^{3+} more tightly, indicate that longer $T_{2,A}$ can be obtained than with nitroxides and thus longer distances can be measured (67).

When performing DEER measurements between a metal center and a nitroxide label, the pump pulse should be applied to the nitroxide (68) to obtain larger inversion efficiency λ. As the electron spin of the metal ion relaxes faster, temperature can be lowered and thus the Boltzmann population difference and sensitivity increased. The technique has been demonstrated for Cu^{2+}-nitroxide (68) and Gd^{3+}-nitroxide (69) pairs and analyzed for peptides labeled with one nitroxide and one Cu^{2+} center (63).

DEER measurements on Gd^{3+}-Gd^{3+} pairs and Gd^{3+}-nitroxide pairs apparently can be analyzed in terms of distances in the same way as measurements between two spin $1/2$ centers. This is no longer true if one center is of non-Kramers type (integer electron spin) and may no longer be true if selective excitation of the $-1/2 \leftrightarrow 1/2$ transition of a high-spin Kramers system is impossible. Dipole-dipole coupling for these more complicated situations has been analyzed theoretically (70).

Another complication occurs for $S = 1/2$ centers with internal electronic structure, such as iron-sulfur centers (71). The point-dipole approximation is poor for the effective spin $1/2$ which arises from antiferromagnetic coupling of three formally $S = 5/2$ spins. Good agreement between expected and measured distance

was obtained by including the spin projection factors into the analysis (72).

3   Information content

3.1   Distance information

3.1.1   MEAN DISTANCES   Due to the dependence of inversion efficiency λ on the ratio between excitation bandwidth and dipole-dipole coupling (22), conformations with very short distances are underrepresented in the DEER signal (73). At standard X-band conditions modulation depth decreases markedly below 2.0 nm. Mean distances shorter than 1.7 nm can hardly be measured reliably (74) unless the distribution is very narrow (49). This lower limit of the sensitive distance range may shift upwards for the more selective pulses often used at Q-band and W-band frequencies and downwards for high-power setups at these frequencies.

The upper limit for obtaining an accurate mean distance can be approximated by $r_{\max,\langle r\rangle} \approx 5\sqrt[3]{t_{\max}/(2\mu s)}$ nm. For the soluble histone core octamer in deuterated buffer good quality data with $t_{\max} \approx 8$ μs were obtained (75), corresponding to a limit of about 8 nm. By deuteration of the same protein $t_{\max}$ could be extended to about 24 μs, corresponding to a limit of about 11.5 nm (29). For membrane proteins in detergent micelles (76) or nanoscale apolipoprotein-bound bilayers (33) $t_{\max} \approx 3.5$ μs can be achieved, putting the limit to about 6 nm. The presence of spin pairs at longer distances can be recognized, but quantitative interpretation of such longer distances should be avoided.

3.1.2   WIDTH OF DISTANCE DISTRIBUTIONS   The width of the distance distribution is encoded in the decay rate of the dipolar oscillations in $F(t)$. Accordingly, several oscillations must be observed for an accurate determination of the width,

which puts the upper limit for such determination to $r_{\mathrm{max},\sigma} \approx 4\sqrt[3]{t_{\mathrm{max}}/(2\mu s)}$. This corresponds to limits of 6 nm for soluble proteins in deuterated buffer, 9 nm for deuterated soluble proteins, and 5 nm for membrane proteins under carefully optimized conditions.

3.1.3 SHAPE OF DISTANCE DISTRIBUTIONS Shapes of distance distributions can be used to characterize conformational distributions (43, 44, 77, 78). The shape of the distance distribution is encoded in the shape of the decay envelope of dipolar oscillation. Upper distance limits for safe interpretation of asymmetries and shoulders of a distribution decrease to 5 nm for soluble proteins in deuterated buffer, 7 nm for deuterated soluble proteins, and only 3.6 nm for membrane proteins. Note however that the presence of several well separated peaks in the distance distribution can be detected up to the limit of reliable detection of the mean distance.

3.2 Number of coupled spins and labeling efficiency

If only one B spin exists in the sensitive distance range of DEER, the modulation depth Δ (Figure 2c) equals the product $p = \lambda f$ of inversion and labeling efficiencies. For $p \ll 1$, the modulation depth in a system of N spins with identical EPR spectra is $(N-1)p$ (3). Relaxing the condition of very small p (79), the number N of spins in a protein or protein complex can be determined from $N = 1 - \ln(1-\Delta)/\ln(1-p)$, provided that f and λ can be estimated independently. Calibration of the constant $C = \ln(1-p)$ with five biradicals and a triradical indicated that N can be measured with an error of less than 0.1 (80). A detailed study on model systems revealed that an additional error in mean spin numbers $\langle N \rangle$ can arise in mixtures of species with different $N > 1$ due to dif-

ferent transverse relaxation times of the species (81). The same study indicated

that $N \leq 4$ can be determined with a precision of 5%. If N is known, the same

method can be used to estimate labeling efficiencies f.

3.3   Angular information (Orientation selection)

From the dependence of $F(t)$ on θ_i the angle between the spin-spin vector and the

ordering direction in a macroscopically ordered sample can be determined, as was

demonstrated on cofactors of photosystem II in oriented thylakoid membranes (9).

For macroscopically disordered samples information on the relative orientation of

the molecular frames of the A and B spins and the spin-spin vector is encoded in

$F(t)$ by orientation selection (42). If the problem is described in molecular frame

A, the five unknown parameters are three Euler angles relating molecular frame B

to frame A and two polar angles specifying the direction of the spin-spin vector in

frame A. It is not currently known what amount of data is required to determine

these five angles uniquely or whether this is possible at all. For the two tyrosyl

radicals in RNR the situation simplifies by C_2 symmetry. Except for a small

displacement that may arise from radical formation a global fit reproduced the

relative tyrosine orientation observed in the crystal structure of the diamagnetic

precursor (82).

   A further complication arises if relative orientation of molecular frames is dis-

tributed, as is usual for nitroxide spin labels (83). Nevertheless, orientation

selection may still be significant at W-band frequencies, so that models for the

distribution of relative orientations can be tested. As has been demonstrated for

particularly rigid spin labels in DNA, angular information can also be obtained

at X-band frequencies (84).

Orientation selection requires selective observer pulses, which may conflict with the excitation bandwidth required for observing short distances. To overcome this problem an observer-selective DEER sequence has been developed (85).

4 Data analysis

4.1 Distances and distance distributions

In mathematical terms the transformation of DEER form factors $F(t)$ to distance distributions $P(r)$ is a moderately ill-posed problem that can be solved by a cross-talk corrected special integral transformation with subsequent distance domain smoothing (13) (Figure 2d). Comparison of several alternative approaches for computation of the distance distribution (86–88) revealed that the best transformation method is Tikhonov regularization with an added non-negativity constraint $P(r) \geq 0$. The optimum regularization parameter can be estimated from the corner of the L curve (Figure 2e) (88). The maximum-entropy method with $P(r) \geq 0$ also performs well, but is comparatively slow (89).

If additional information on the shape of the expected distribution is available, model-based fitting of $P(r)$ can be preferable (90). Fast integral transformation, Tikhonov regularization with $P(r) \geq 0$, and model-based fitting are incorporated into the software package DeerAnalysis (91), which also provides several ways of separating the primary DEER data into $F(t)$ and $B(t)$. Note that a Gaussian distribution of spin label positions leads to a Rice distribution of interspin distances (92), a fact that may be important for consistent analysis of triangulation data from several spin pairs.

4.2   Distance changes

In many applications reliable detection of small distance changes between states 1 and 2 of a protein is important. Since transformation of the form factor $F(t)$ to the distance distribution $P(r)$ is ill-posed, it is hard to ascertain whether changes in $P(r)$ are significant. Significant change implies that the primary data $V_1(t)$ and $V_2(t)$ as well as the form factors $F_1(t)$ and $F_2(t)$ differ. Since the two samples may have different labeling efficiency f or different concentration, comparison may require scaling to the same modulation depth Δ. The scaling of primary data needs to be done on $\log V_i(t)$ to correct for concentration differences, whereas the $F_i(t)$ need to be scaled linearly to avoid distortion of the distance distribution. Such comparison is included as a dual display feature in DeerAnalysis (91).

4.3   Orientation selection

Orientation selection was analyzed for high-frequency DEER with enhanced symmetry of the relative orientation without (82) and with (83) conformational distribution of the paramagnetic center and for general symmetry for a cofactor pair in photosynthetic reaction centers (93). Analysis at X-band frequencies was desccribed for Cu^{2+}-Cu^{2+} (63, 94), Cu^{2+}-nitroxide (63, 64) and iron-sulfur centre-nitroxide (94) pairs. In the last case spin projection factors were taken into account.

   Model-free analysis of orientation selection can be achieved by subjecting form factors $F_i(t)$ obtained at different observer/pump frequency settings i to two Tikhonov regularization steps (45). In the first step $\sum_i F_i(t)$ is converted to the distance distribution $P(r)$. In the second step orientation distributions $P_i(\theta)$ are determined from the individual $F_i(t)$ and from $P(r)$. If the hyperfine and g

tensor of both the A and B spin can be approximated with axial symmetry and if the unique axes of all four tensors are parallel, geometry is characterized by a single angle β between the spin-spin vector and the coinciding unique axes of the molecular frames A and B. For this case an analytical expression relates β to the value of the observer frequency at which $P(\theta_i)$ assumes its maximum (95).

5 Relation of label-to-label distances to protein structure

5.1 Spin label conformation

DEER distance constraints can be interpreted in terms of protein structure only by taking into account the conformation of the spin label (16). The first systematic explicit treatment of spin label conformational distribution used a combination of Monte Carlo conformational search and short molecular dynamics (MD) computations (96). Compared to modeling by the C^β-C^β distance this approach significantly improved agreement between experimental and theoretical distances for potassium channel KcsA and troponin C. Fast and convenient predictions are possible by rotamer library modeling of the conformational space, i.e. by assuming a small number of canonical values for each of the dihedral angles (Figure 4a) of the side chain (97). In the current approach the interaction energy of each spin label rotamer with backbone atoms and neighboring sidegroups is computed from only a Lennard-Jones potential (6). For lack of a sufficiently large experimental data base of spin label conformations, the most recent rotamer libraries are still calibrated by long MD runs (98). For three pairs between a flavin adenine dinucleotide cofactor radical and a nitroxide spin label in acyl-CoA dehydrogenase full MD simulations were found to be in good agreement with rotamer library predictions, whereas results of DEER measurements differed from both, indicat-

ing structural flexibility of the protein backbone (36). An even simpler modeling approach that does not include Boltzmann weighting of rotamers, but only removal of clashing conformations, was found to be in good agreement with two distance measurements on azurin (99).

Good agreement between such predictions and experiment should not be taken for granted, however. Current modeling procedures may fail to account for subtle effects, such as occasional conformational change of the spin label upon freezing, which is caused by changes in hydrophobic effects (100). Furthermore, label sidechains appear to have a strong preference for hydrophobic pockets, which may lead to deviations of the dihedral angles from the canonical values encountered in MD simulations (101). Deviations between rotamer library predictions and experiment are most likely for narrow distance distributions, such as the one between MTSL at residues 202 and 202' in sodium/proton antiporter NhaA of *Escherichia coli* (Figure 4b-d). Note that the significant deviation of the experimental distance distribution from the one predicted from structural model 3FI1 (102) (Figure 4c) corresponds to only a minor difference in the primary data (Figure 4d). Hence, despite the prediction uncertainty the relative arrangement of monomers in the NhaA dimer could be determined with rather good resolution by directly fitting primary data (97,98). Experimental distance distributions and, by implication, spin label conformations appear to be rather insensitive to the choice of cryoprotectant (103).

Crystal structures of several T4 lysozyme mutants labeled with MTSL exhibit resolved electron density for at least the first few atoms of the MTSL side chain (104). Analysis suggests a preference for conformations with close contact of the S^δ atom with the backbone, which is possibly not fully accounted for in

current MD simulations. For an MTSL spin label attached to residue 55 of the homodimeric protein CylR2 a single conformation is observed in the x-ray structure, which was compared with NMR paramagnetic relaxation enhancement data in solution and a DEER distance measurement in frozen solution (105). Agreement for the NMR data is very good, whereas the mean distance determined by DEER is 0.16 nm shorter than the one in the crystal structure.

5.2 Modeling of structures with sparse distance constraints

The current SDSL approach provides one distance constraint per protein sample. As a consequence, the number of distance constraints in DEER studies is much smaller than the number of backbone dihedrals in proteins. Such sparse distance constraints have been used for modeling of possible sites of the N terminus of light harvesting complex II at low resolution (19). Distance constraints were specified with respect to the O^γ and C^γ atoms of the native serine and valine residues at the labeling sites and used to restrain loop models generated by the Modeller (106) software.

In determination of relative arrangments of components of a protein complex the sparsity problem does not arise if the component structures are known and can be treated as rigid bodies. To model the relative arrangement of the CheW-P5 complex, the x-ray structures of the two moieties and 12 label-to-label distance constraints as soft-square potential C^β-C^β restraints were supplied to the CNS (107) software and the best-fitting rigid-body transformation was established (108, 109). Relative arrangement of monomers in the NhaA homodimer of the sodium/proton antiporter NhaA could be determined from nine label-to-label constraints and the crystal structure of the monomer (97). The nine distance

measurements overdetermine the problem posed as a rigid-body transformation with C_2 symmetry (Figure 5a), which has only four free parameters. Primary DEER data were directly fitted (see also Figure 3c) and the whole possible range of the four free parameters was scanned in a grid search. As discussed in (98), the dimer structure was later confirmed by electron crystallography, except for the position of two contacting β-sheets that had undergone a conformational change due to crystal packing. This illustrates scope and limitations of the rigid-body approximation.

If this approximation cannot be made, structures obtained from sparse constraints are necessarily either coarse-grained or uncertain. Coarse-grained (two particles per residue) Monte Carlo simulations of the 26-residue antimicrobial peptide melittin were applied to study interaction of this peptide with a lipid bilayer (110). The crystal structure of melittin was used as a starting conformation and MTSL was mimicked by leucine. Four DEER distance distributions and five water accessibility parameters from electron spin echo envelope modulation (ESEEM) spectroscopy were used as constraints. The peptide was found in a primarily α-helical conformation oriented mainly parallel to the membrane.

The shape of the 28-residue transmembrane domain (TMD) IX of the proline/sodium symporter PutP was modeled by a coarse-grained helix-loop-helix construct (111). Out of 16 DEER measurements, twelve could be used as distance constraints and four as lower-bound restraints. In agreement with residue accessibility data, a pronounced kink of TMD IX was found.

Since atomistic models can be stabilized by force fields, it is also possible to perform atomistic MD simulations that are biased by DEER distance constraints. Such an approach was applied to specify the structure of an 82-residue membrane

bound fragment of α-synuclein (112). Accessibility data indicated helical structure for the whole stretch of residues, which made it reasonable to start simulated annealing MD simulations from an ideal α-helix. By explicitly including MTSL and using 14 DEER distances constraints and three lower-bound restraints the residue stretch was found to be an extended, slightly curved α-helix. This approach was later extended by considering α-synuclein as partially unfolded and describing it in terms of a structural ensemble (113). Using distance distribution information from 18 spin pairs together with NMR secondary structure restraints and bond vector restraints, a minimal set of basis structures was derived. Spin label conformations were restricted to the five rotameric states of the first three sidechain dihedral angles that had been previously observed in crystal structures for surface-exposed MTSL in an α-helical context, while the remaining two dihedral angles were allowed to vary.

A few DEER long-range distance constraints can facilitate NMR structure determination in cases that are problematic without such constraints. Relative orientation of the domains in the polypeptide transport-associated protein BamA was studied by a combination of DEER and NMR techniques (114). The two domains are only loosely connected, so that only three out of 2709 NMR nuclear Overhauser enhancement distance constraints are interdomain constraints. These three short-range constraints are insufficient for specifying relative domain orientation. Only three additional DEER long-range distance constraints fixed this orientation reasonably well in MD simulations. A similar approach was used to solve the homodimer structure of the 52-residue protein Dsy0195, which is involved in spore coat assembly during the process of sporulation of *Desulfitobacterium hafniense* (115). By using two DEER distance constraints and NMR

paramagnetic relaxation enhancement (PRE) data from the same MTSL labels as constraint seeds, structure determination of this homodimer became possible, while it failed without the MTSL-based constraints. The structure was confirmed by x-ray crystallography.

The general problem of sparse distance constraints was addressed in a theoretical study (117). Although the study focused on short-range (NMR type) constraints, the results provide a semi-quantitative estimate of how uncertainty of the structure, measured as root mean square deviation from the native structure, increases when the number of constraints is reduced. The problem of *de novo* structure modeling from sparse EPR distance constraints without recourse to constraints from other techniques is addressed by an approach (118) based on Rosetta (116). Spin labels were integrated by a 'motion-in-a-cone' model (119). Model quality after the initial folding step improved markedly for the α-helical core domain of T4 lysozyme (residues 58–164) when including 25 distance constraints from CW EPR and DEER measurements (118).

Structure characterization based on sparse DEER constraints crucially depends on optimum site pair selection. If the structure of a homologous protein or the same protein in a different state is known, site pairs can be selected by the Zheng/Brooks algorithm (120), which is based on fluctuation analysis with an elastic network model. The same study showed that iterative fitting of only ten distance constraints by transformation along reoriented normal modes of an elastic network model can provide good models for structural transitions of proteins with about 300 residues. For the maltose binding protein MalE, one of the examples in this study, the structural transition and selected site pairs are visualized in Figure 5b. For MalE all optimally selected constraints fall in the

range accessible by DEER, in some of the other cases one or two constraints are at shorter distances accessible by CW EPR.

Selection of spin labeling sites is also restricted by the requirements for sufficient accessibility and avoidance of structural distortion. Spin labeling site scans with the rotamer library approach can provide information on tight sites, where labeling may fail or distort structure, and very loose sites where broad conformational distributions are expected (121). Spin-labeling site scans in MMM (47) allow to restrict labeling sites to user-selected types of residues. For *de novo* protein structure determination a site-pair selection algorithm was proposed, too (122).

6 Selected further applications

6.1 Semi-quantitative topology model

The protein TonB is supposed to transfer energy generated from the proton motive force across the inner bacterial membrane to outer membrane receptors. Topology of TonB was addressed by measuring six distances in a segment between residues 59 and 120 (123). The pairs of labeling sites were selected in this range and spaced by six to 17 residues, so that all distances fell into the most sensitive DEER range between 2.5 and 4.6 nm. The data supported an extended polyproline II-like conformation, which agrees with the high proline content of the segment and the requirement for TonB to span the periplasm.

6.2 Ligand binding

The most abundant protein in human blood plasma, human serum albumin (HSA), is a promiscuous transporter that binds, among else, fatty acids. The

distribution of up to six fatty acid ligands was studied by adding 5-doxyl- or 16-doxyl-stearic acid to the apoprotein and measuring the distance distributions between the labels (124). Experimental data revealed a much more symmetric distribution of the ligands than had been previously observed in a crystal structure of the HSA complex with fatty acids, in particular for the hydrophobic chain end at position 16. Addition of the ionic liquid choline dihydrogenphosphate results in a distribution closer to the one expected from the crystal structure, probably due to rigidification of the protein surface and hydrophobic chain ends (125). Choline dihydrogenphosphate is added to crystallization buffers to stabilize protein structure, but according to this study it may artificially rigidify proteins.

6.3 Conformational changes

The visual pigment rhodopsin undergoes a conformational change on light activation that was suggested to involve an outward tilt of TMD 6. An extensive DEER triangulation was performed by measuring 16 distances between labeling sites addressing residues 241 and 252 in TMD 6, one residue near the cytoplasmic face of each of the other six TMDs, and one residue in the cytoplasmic helix H8 (126). This scheme allowed visualization of the label positions as density clouds in the context of the crystal structure of the inactive state. The same distances were then measured for the activated state and the structural change was discussed from the observed shifts of the density clouds. The motion of TMD6 was found to be an outward movement by about 5 Å.

Peptide binding to the ATP-binding cassette (ABC) transporter associated with antigen processing (TAP) was studied with peptides with a length of 7, 9,

and 15 residues that were labeled with iodo-acetamido proxyl at the second and second-to-last residue (127). TAP binds peptides with a length of 8–16 residues with comparable affinity. For the 9-mer, binding merely lead to a sharpening of the distance distribution, while for the 15-mer, sharpening of the distribution and shortening of the distance were observed. Very similar distance distributions were observed for the peptides bound to TAP and to an MHC class I molecule that transports peptides to the cell surface to display them as antigens. This suggests binding of peptides in the same conformation by TAP and MHC class I molecules, consistent with coevolution of these two parts of the antigen-processing machinery.

The motor protein myosin generates a force on actin during muscle contraction by changing its structure forth and back to generate a power stroke and recovery stroke. The energy for these changes stems from ATP binding and hydrolysis. A series of crystal structures identified a rotation of the relay helix relative to the catalytic domain as an important component of the structural change. Structural dynamics of the relay helix was addressed by a combined DEER and time-resolved fluorescence resonance enery transfer (FRET) approach (128). Distance distributions between a site on the C terminus of the relay helix and two sites in one of the stable helices in the lower 50K domain were measured in the absence and presence of ADP and nucleotide analogs. The results suggest two-state behavior of the relay helix. The minor effects of ADP binding were barely significant in DEER measurements and not detectable by FRET. In contrast, the ATP analog ADP·BeF$_x$ effects a strong change, which can be observed by both techniques and was more precisely quantyified by DEER. This suggests that ATP binding rather than ATP hydrolysis induces the recovery stroke.

Myosin II is allosterically regulated by phosphorylation of a single serine of each of the two regulatory light chains. This regulation is supposed to be due to a redistribution of fractional populations of distinct conformational substates, which can dynamically interchange even in the absence of the allosteric ligand. This hypothesis was tested by analyzing DEER data in terms of a minimum number of Gaussians (129). Indeed two populations were detected in unphosphorylated myosin II and one of them was suppressed by phosphorylation. By attributing the narrower distributions to the off state, a coarse-grained model of the off and on state structures could be created from the crystal structure of smooth muscle myosin by a rigid docking approach. This work nicely illustrates the utility of DEER for characterization of proteins that exhibit conformational heterogeneity.

Secondary transporters, such as lactose permease LacY utilize electrochemical gradients of protons or sodium ions for transport of nutrients against a concentration gradient. This is usually explained by an alternating access model, which requires conformational change between an inward-facing and an outward-facing conformation. All x-ray structures of LacY correspond to the same inward-facing conformation. The outward-facing conformation could be detected by sugar binding to LacY in micellar solution, with distances generally shortening on the cytoplasmic side and lengthening on the periplasmic side (130).

The outer membrane of bacteria includes a class of active transport proteins which depend on TonB, are based on a 22-stranded β-barrel, and transport a variety of substrates. A large extracellular loop binds the ligand. Binding of Ca^{2+}, vitamin B_{12}, and polyethylene glycol (PEG) to the vitamin B_{12} transporter BtuB was studied by DEER (131). Distance distributions between site T188 at the apex of loop 2 and three residues on the outer rim of the β-barrel strongly narrow and

slightly shift on binding of Ca^{2+}, indicating that calcium binding orders and rigidifies the loop. Addition of PEG to the Ca^{2+}-bound species changes the distance distributions, thus demonstrating that this ubiquitous component of membrane protein crystallization cocktails is not innocent and may prevent observation of functionally relevant substrate binding.

6.4 Large-scale domain movements

The crystal structure of the G protein MnmE involved in posttranscriptional modification of transfer RNA suggested a tendency for dimerization. A dimer model created from this crystal structure was tested by DEER measurements in frozen solution on four singly spin-labeled mutants addressing the $G\alpha 2$, the $G\alpha 5$, the switch II, and the N-terminal domains (132). The apoprotein dimer exhibits an open structure in solution, similar to the one predicted from the crystal structure. No dramatic changes were observed by adding GDP. In contrast, addition of the non-hydrolyzable GTP analog GppNHp leads to occurence of a second, closed conformation, which appears to be in thermal equilibrium with the open conformation. Addition of the transition-state mimic GDP·AlF$_x$ seems to stabilize exclusively the closed conformation. Interestingly, only K^+ ions, which are known to activate MnME GTPase, but not the smaller Na^+ or much larger Cs^+ ions, are able to stabilize the closed state. This K^+ dependence is abolished by complexation of MnmE with the FAD-binding protein GidA, which is required for modification of some particular transfer RNAs (133).

Maturing and infectiousness of Human Immunodeficiency Virus (HIV) crucially depend on activity of HIV-1 protease, which is thus an important drug target. Under protease inhibitor drug pressure mutations evolve to evade these inhibitors,

probably by altering conformation of the flaps that open and close the active site. This hypothesis was tested by a combined approach of DEER measurements and 30 ns MD simulations at 300 K in explicit solvent, including MTSL (134). Although the study is based on only one mutant and no special care was taken in sampling of spin label conformations, the trends in the distance distributions revealed by DEER are in astonishing agreement with the MD results. This shows that a small number of DEER measurements can lend support to results of MD approaches and, in this particular case, that HIV evades protease inhibitor drugs by narrowing the conformational distribution of the flaps.

6.5   Complex formation and structure

DEER can observe dipole-dipole interaction between spin labels in two molecules even if complex formation is incomplete and transient and can thus be used to detect and quantify oligomerization equilibria. Sodium/proton antiporter NhaA, which is crucial for Na^+ homeostatis in bacteria at high environmental salt concentrations, appears to form a dimer under physiological conditions, although the transport pathway is in the center of the monomeric protein. The hypothesis that pH-dependence of the activity of NhaA is due to pH-dependence of the dimerization equilibrium was rejected by DEER measurements (80). The mean number of spins per object, as derived from the modulation depth Δ, was found to depend only weakly on pH.

Monoamine oxidases (MAO) are required for oxidative deamination of amine neurotransmitters and dietary amines. While human hMAOA crystallized as a monomer the corresponding rat rMAOA crystallized as a dimer. Based on sequence conservation analysis it was suggested that a human exclusive mutation

E151K destabilizes the dimer interface in hMAOA. This hypothesis was rejected by DEER measurements between nitroxide labeled pargyline inhibitors and between flavine semiquinone anion radicals (135). The results suggest very similar dimeric structures for hMAOA and rMAOA in both the inhibited and uninhibited form, if these proteins are bound to outer mitochondrial membranes. The occurence of hMAOA as a monomer in the x-ray structure is probably induced by the octyl β–D–pyranoside (OGP) micelles used for crystallization.

6.6 Special applications

The electron transfer protein RNR harbors a stable tyrosyl radical cofactor Y122, which is essential for catalysis, yet remote from the active site located at a different center. While it is clear that the radical state must be propagated over about 3.5 nm for the protein to function, the radical transfer pathway could not be mapped due to the transient nature of putative intermediate radical states at Y356, Y730, and Y731. This problem was addressed by engineering radical traps by modification of Y356 to 3-hydroxytyrosine and of Y731 to 3-aminotyrosine (136). Distances between the engineered stable radicals measured by DEER are consistent with a docking model for the homodimeric RNR $\alpha 2$ and $\beta 2$ subunits and modulation depths are consistent with a half-site reactivity model, where during first turnover only one of the two symmetry-related radical transfer pathways is used.

The width of DEER distance distributions was analyzed in terms of molecular-scale force between domains in an α-helical coiled-coil leucine zipper structure (137). TOAC spin labels were applied, so that contributions from the conformational distribution of the label could be neglected. An intercoil force of 110 ± 10

pN was derived from the DEER data, while MD calculations at 298 K gave 90 ± 10 pN. The difference could be explained by reasoning that the force measured by DEER in glassy frozen solution should correspond to the glass transition temperature of the matrix, a proposition that was later tested and confirmed for shape-persistent polymers (44).

Access to disordered proteins by DEER allows for studies of protein folding by freeze-quench techniques, as was demonstrated on self-assembly of LHCII from the unfolded apoprotein, pigments, and lipids (53). Although strong changes in the primary DEER data were observed for both site pairs during folding, short relaxation times in the unfolded state precluded analysis in terms of the distance distribution. This problem was solved by analyzing dipolar spectra, which can be obtained by Fourier transformation of $F(t)$. Superposition of normalized dipolar spectra revealed isosbestic points for both site pairs, encouraging analysis in terms of a first-order kinetic transition between two states. Analysis of depletion of the shortest distances revealed that formation of transmembrane helix 3 is faster than relative arrangement of the two intertwined transmembrane helices 1 and 4.

7   Summary Points list

1. DEER accesses a distance range from about 1.8 to 5 or 10 nm, depending on protein type and environment; this matches typical protein dimensions.

2. DEER measurements can typically be made at 100 μM protein concentration with about 50 μL of sample volume on commercial X-band spectrometers. The best home-built spectrometers at Q- and W-band frequencies perform better by at least one order of magnitude on both counts.

3. The number of paramagnetic centers per protein molecule or protein com-

plex can be estimated and, in favorable cases, information on relative orientation of radical cofactors can be obtained.

4. Errors introduced by approximations in the conversion from primary experimental data to distance distributions are usually negligible compared to the uncertainty in modeling the distribution of spin label conformation.

5. Specification of an atomistic structure from only DEER distance constraints is unrealistic due to the expense involved in obtaining a sufficient number of constraints. The sparse constraint set can fully specify rigid-body movements, can guide coarse-grained or atomistic MD simulations as well as Rosetta structure predictions, and can complement incomplete constraint lists from NMR spectroscopy.

6. DEER is particularly well suited for addressing partially disordered domains, structural changes on ligand or cofactor binding, large-scale domain movements, and formation of protein complexes that are hard to crystallize and too large for high-resolution NMR spectroscopy. As any application of SDSL EPR, DEER excels on membrane proteins that can be studied in more physiological environments than with most other techniques.

7. Access to a distance distribution rather than only a single number for the distance allows to quantify flexibility of structures and to follow disorder-to-order transitions such as protein folding.

8 Future issues

1. The commercial spectrometers used by most practitioners in the field have the scope to achieve 5 μM sensitivity with 4 μL of sample volume, if state-

of-the-art power amplifiers are used at Q-band frequency. At the expense of requiring more sample volume, even better concentration sensitivity is feasible with dedicated probeheads for oversized samples. This would ease background correction and protein aggregation problems.

2. Better understanding of orientation selection should lead to better ways of controlling it. In many applications, full suppression of this effect is desirable. Furthermore, experimental protocols are needed that provide maximum information on relative orientation with a minimum number of measurements. Data analysis procedures should be developed that fully account for possible ambiguities in fitting experimental data.

3. Extension to longer distances relies on reducing transverse relaxation. Development of different types of labels and a better understanding of the dependence of nuclear spin diffusion effects on label environment are possible routes.

4. The increasing database on distance distributions in systems with known structure and on spin label conformations in protein crystals should be used to improve modeling of the conformational distribution of spin labels. In particular, an algorithm is needed for recognizing hydrophobic cavities where a label can fit in with only small structural perturbation.

5. Uncertainty in modeling structures and structural transitions from a list of sparse distance constraints needs to be better understood. Modeling approaches are required that can supplement DEER distance constraints by other constraints available with SDSL techniques, for instance by constraints on secondary structure or label accessibility.

9 Acknowledgment

10 Literature cited

LITERATURE CITED

1. Kaplan DE, Hahn EL. 1958. Experiences de double irradiation en resonance magnetique par la méthode d'impulsions. *J. Phys. Rad.* 19:821–5.

2. Milov AD, Salikhov KM, Shchirov MD. 1981. Use of the double resonance in electron spin echo method for the study of paramagnetic center spatial distribution in solids. *Fiz. Tverd. Tela (Leningrad)* 23:975–82.

3. Milov AD, Ponomarev AB, Tsvetkov YD. 1984. Electron-electron double resonance in electron spin echo: model biradical systems and the sensitized photolysis of decalin. *Chem. Phys. Lett.* 110:67–72.

4. Martin RE, Pannier M, Diederich F, Gramlich V, Hubrich M, Spiess HW. 1998. Determination of end-to-end distances in a series of TEMPO diradicals of up to 2.8 nm length with a new four-pulse double electron electron resonance experiment. *Angew. Chem. Int. Ed.* 37:2834–2837.

5. Pannier M, Veit S, Godt A, Jeschke G, Spiess HW. 2000. Dead-Time Free Measurement of Dipole-Dipole Interactions between Electron Spins. *J. Magn. Reson.* 142:331–340.

6. Jeschke G, Polyhach Y. 2007. Distance measurements on spin-labelled biomacromolecules by pulsed electron paramagnetic resonance. *Phys. Chem.*

Chem. Phys. 9:1895–1910.

7. Schiemann O, Prisner TF. 2007. Long-range distance determinations in biomacromolecules by EPR spectroscopy. *Q. Rev. Biophys.* 40:1–53.

8. Tsvetkov YD, Milov AD, Maryasov AG. 2008. Pulsed electron-electron double resonance (PELDOR) as EPR spectroscopy in nanometre range. *Russ. Chem. Rev.* 77:487–520.

9. Astashkin AV, Hara H, Kawamori A. 1998. The pulsed electron-electron double resonance and "2+1" electron spin echo study of the oriented oxygen-evolving and Mn-depleted preparations of photosystem II. *J. Chem. Phys.* 108:3805–3812.

10. Todd AP, Cong J, Levinthal F, Levinthal C, Hubbell WL. 1989. Site-directed mutagenesis of colicin E1 provides specific attachment sites for spin labels whose spectra are sensitive to local conformation. *Proteins: Struct,. Funct,. Genet.* 6:294–305.

11. Hubbell WL, Cafiso DS, Altenbach C. 2000. Identifying conformational changes with site-directed spin labeling. *Nat. Struct. Biol.* 7:735–9.

12. Borbat PP, Freed JH. 1999. Multiple-quantum ESR and distance measurements. *Chem. Phys. Lett.* 313:145–154.

13. Jeschke G, Koch A, Jonas U, Godt A. 2002. Direct conversion of EPR dipolar time evolution data to distance distributions. *J. Magn. Reson.* 155:72–82.

14. Milov AD, Maryasov AG, Tsvetkov YD, Raap J. 1999. Pulsed ELDOR in spin-labeled polypeptides. *Chem. Phys. Lett.* 303:135–143.

15. Persson M, Harbridge JR, Hammarstrom P, Mitri R, Martensson LG *et al.* 2001. Comparison of electron paramagnetic resonance methods to determine distances between spin labels on human carbonic anhydrase II. *Biophys. J.*

80:2886–2897.

16. Borbat PP, Mchaourab HS, Freed JH. 2002. Protein Structure Determination Using Long-Distance Constraints from Double-Quantum Coherence ESR: Study of T4 Lysozyme. *J. Am. Chem. Soc.* 124:5304–5314.

17. Bennati M, Weber A, Antonic J, Perlstein DL, Robblee J, Stubbe J. 2003. Pulsed ELDOR spectroscopy measures the distance between the two tyrosyl radicals in the R2 subunit of the E. coli ribonucleotide reductase. *J. Am. Chem. Soc.* 125:14988–9.

18. Jeschke G, Wegener C, Nietschke M, Jung H, Steinhoff H. 2004. Interresidual distance determination by four-pulse double electron-electron resonance in an integral membrane protein: the Na+/proline transporter PutP of Escherichia coli. *Biophys. J.* 86:2551–2557.

19. Jeschke G, Bender A, Schweikardt T, Panek G, Decker H, Paulsen H. 2005. Localization of the N-terminal Domain in Light-harvesting Chlorophyll a/b Protein by EPR Measurements. *J. Biol. Chem.* 280:18623–18630.

20. Milov AD, Maryasov AG, Tsvetkov YD. 1998. Pulsed electron double resonance (PELDOR) and its applications in free-radicals research. *Appl. Magn. Reson.* 15:107–143.

21. Jeschke G, Spiess HW. 2006. Distance measurements in solid-state NMR and EPR spectroscopy. *Lect. Notes Phys.* 684:21–63.

22. Maryasov AG, Tsvetkov YD. 2000. Formation of the pulsed electron-electron double resonance signal in the case of a finite amplitude of microwave fields. *Appl. Magn. Reson.* 18:583–605.

23. Bowman MK, Maryasov AG. 2007. Dynamic phase shifts in nanoscale distance measurements by double electron electron resonance (DEER). *J. Magn.*

Reson. 185:270–282.

24. Milov AD, Tsvetkov YD. 1997. Double electron-electron resonance in electron spin echo: Conformations; of spin-labeled poly-4-vinilpyridine in glassy solutions. *Appl. Magn. Reson.* 12:495–504.

25. Jeschke G, Sajid M, Schulte M, Godt A. 2009. Three-spin correlations in double electron-electron resonance. *Phys. Chem. Chem. Phys.* 11:6580–6591.

26. Jeschke G, Pannier M, Godt A, Spiess HW. 2000. Dipolar spectroscopy and spin alignment in electron paramagnetic resonance. *Chem. Phys. Lett.* 331:243–252.

27. Hara H, Tenno T, Shirakawa M. 2007. Distance determination in human ubiquitin by pulsed double electron-electron resonance and double quantum coherence ESR methods. *J. Magn. Reson.* 184:78–84.

28. Jeschke G, Bender A, Paulsen H, Zimmermann H, Godt A. 2004. Sensitivity enhancement in pulse EPR distance measurements. *J. Magn. Reson.* 169:1–12.

29. Ward R, Bowman A, Sozudogru E, El-Mkami H, Owen-Hughes T, Norman DG. 2010. EPR distance measurements in deuterated proteins. *J. Magn. Reson.* 207:164–167.

30. Endeward B, Butterwick JA, MacKinnon R, Prisner TF. 2009. Pulsed electron-electron double-resonance determination of spin-label distances and orientations on the tetrameric potassium ion channel KcsA. *J. Am. Chem. Soc.* 131:15246–50.

31. Dastvan R, Bode BE, Karuppiah MPR, Marko A, Lyubenova S *et al.* 2010. Optimization of Transversal Relaxation of Nitroxides for Pulsed Electron-Electron Double Resonance Spectroscopy in Phospholipid Membranes. *J.*

Phys. Chem. B. 114:13507–13516.

32. Alvarez FJD, Orelle C, Davidson AL. 2010. Functional Reconstitution of an ABC Transporter in Nanodiscs for Use in Electron Paramagnetic Resonance Spectroscopy. *J. Am. Chem. Soc.* 132:9513–9515.

33. Zou P, Mchaourab HS. 2010. Increased sensitivity and extended range of distance measurements in spin-labeled membrane proteins: Q-band double electron-electron resonance and nanoscale bilayers. *Biophys. J.* 98:L18–L20.

34. Höfer P, Heilig R, Maier DC, Prisecaru I, Schmalbein D. 2003. The superQ-FT accessory for pulsed EPR, ENDOR and ELDOR at 34 GHz. *Bruker SpinReport* 152/153:37–43.

35. Ghimire H, McCarrick RM, Budil DE, Lorigan GA. 2009. Significantly Improved Sensitivity of Q-Band PELDOR/DEER Experiments Relative to X-Band Is Observed in Measuring the Intercoil Distance of a Leucine Zipper Motif Peptide (GCN4-LZ). *Biochemistry* 48:5782–5784.

36. Swanson MA, Kathirvelu V, Majtan T, Frerman FE, Eaton GR, Eaton SS. 2011. Electron transfer flavoprotein domain II orientation monitored using double electron-electron resonance between an enzymatically reduced, native FAD cofactor, and spin labels. *Protein. Sci* 20:610–20.

37. Tschaggelar R, Kasumaj B, Santangelo MG, Forrer J, Leger P *et al.* 2009. Cryogenic 35 GHz pulse ENDOR probehead accommodating large sample sizes: Performance and applications. *J. Magn. Reson.* 200:81–87.

38. Biglino D, Schmidt PP, Reijerse EJ, Lubitz W. 2006. PELDOR study on the tyrosyl radicals in the R2 protein of mouse ribonucleotide reductase. *Phys. Chem. Chem. Phys.* 8:58–62.

39. Song L, Larion M, Chamoun J, Bonora M, Fajer PG. 2009. Distance and

dynamics determination by W-band DEER and W-band ST-EPR. *Eur. Biophys. J.* 39:711–9.

40. Cruickshank PA, Bolton DR, Robertson DA, Hunter RI, Wylde RJ, Smith GM. 2009. A kilowatt pulsed 94 GHz electron paramagnetic resonance spectrometer with high concentration sensitivity, high instantaneous bandwidth, and low dead time. *Rev. Sci. Instrum.* 80:103102.

41. Denysenkov VP, Prisner TF, Stubbe J, Bennati M. 2005. High-frequency 180 GHz PELDOR. *Appl. Magn. Reson.* 29:375–384.

42. Larsen RG, Singel DJ. 1993. Double electron-electron resonance spin-echo modulation: spectroscopic measurement of electron spin pair separations in orientationally disordered solids. *J. Chem. Phys.* 98:5134–46.

43. Godt A, Schulte M, Zimmermann H, Jeschke G. 2006. How flexible are poly(para-phenyleneethynylene)s?. *Angew. Chem. Int. Ed.* 45:7560–7564.

44. Jeschke G, Sajid M, Schulte M, Ramezanian N, Volkov A *et al.* 2010. Flexibility of Shape-Persistent Molecular Building Blocks Composed of p-Phenylene and Ethynylene Units. *J. Am. Chem. Soc.* 132:10107–10117.

45. Marko A, Margraf D, Yu H, Mu Y, Stock G, Prisner T. 2009. Molecular orientation studies by pulsed electron-electron double resonance experiments. *J. Chem. Phys.* 130:064102/1–064102/9.

46. Kurshev VV, Raitsimring AM, Tsvetkov YD. 1989. Selection of dipolar interaction by the "2 + 1" pulse train ESE. *J. Magn. Reson.* 81:441–54.

47. Jeschke G, Polyhach Y, Bordignon E. 2010. *Multiscale Modeling of Marcomolecules – MMM.* ETH Zürich. http://www.epr.ethz.ch/software/index.

48. Jeschke G. 2002. Determination of the nanostructure of polymer materials by electron paramagnetic resonance spectroscopy. *Macromol Rapid. Commun.*

23:227–246.

49. Weber A, Schiemann O, Bode B, Prisner TF. 2002. PELDOR at S- and X-Band Frequencies and the Separation of Exchange Coupling from Dipolar Coupling. *J. Magn. Reson.* 157:277–285.

50. Riplinger C, Kao JPY, Rosen GM, Kathirvelu V, Eaton GR *et al.* 2009. Interaction of Radical Pairs Through-Bond and Through-Space: Scope and Limitations of the Point-Dipole Approximation in Electron Paramagnetic Resonance Spectroscopy. *J. Am. Chem. Soc.* 131:10092–10106.

51. Berliner LJ, Grunwald J, Hankovszky HO, Hideg K. 1982. A novel reversible thiol-specific spin label: papain active site labeling and inhibition. *Anal. Biochem.* 119:450–5.

52. Igarashi R, Sakai T, Hara H, Tenno T, Tanaka T *et al.* 2010. Distance determination in proteins inside Xenopus laevis oocytes by double electron-electron resonance experiments. *J. Am. Chem. Soc.* 132:8228–9.

53. Dockter C, Volkov A, Bauer C, Polyhach Y, Joly-Lopez Z *et al.* 2009. Refolding of the integral membrane protein light-harvesting complex II monitored by pulse EPR. *Proc. Natl. Acad. Sci U. S. A.* 106:18485–90.

54. Couet WR, Brasch RC, Sosnovsky G, Tozer TN. 1985. Factors affecting nitroxide reduction in ascorbate solution and tissue homogenates. *Magn. Reson. Imaging.* 3:83–8.

55. Fleissner MR, Brustad EM, Kalai T, Altenbach C, Cascio D *et al.* 2009. Site-directed spin labeling of a genetically encoded unnatural amino acid. *Proc. Natl. Acad. Sci U. S. A.* 106:21637–21642.

56. Nakaie CR, Schreier S, Paiva ACM. 1983. Synthesis and properties of spin-labeled angiotensin derivatives. *Biochim. Biophys. Acta Protein. Struct. Mol.*

Enzymol. 742:63–71.

57. Marchetto R, Schreier S, Nakaie CR. 1993. A novel spin-labeled amino acid derivative for use in peptide synthesis: (9-fluorenylmethyloxycarbonyl)-2,2,6,6-tetramethylpiperidine-N-oxyl-4-amino-4-carboxylic acid. *J. Am. Chem. Soc.* 115:11042–3.

58. Toniolo C, Valente E, Formaggio F, Crisma M, Pilloni G *et al.* 1995. Synthesis and conformational studies of peptides containing TOAC, a spin-labelled C alpha, alpha-disubstituted glycine. *J. Pept. Sci.* 1:45–57.

59. Rajca A, Kathirvelu V, Roy SK, Pink M, Rajca S *et al.* 2010. A spirocyclohexyl nitroxide amino acid spin label for pulsed EPR spectroscopy distance measurements. *Chem. Eur. J.* 16:5778–82.

60. Jeschke G, Zimmermann H, Godt A. 2006. Isotope selection in distance measurements between nitroxides. *J. Magn. Reson.* 180:137–146.

61. van Amsterdam IM, Ubbink M, Canters GW, Huber M. 2003. Measurement of a Cu-Cu distance of 26 A by a pulsed EPR method. *Angew. Chem. Int. Ed. Engl.* 42:62–4.

62. Kay CW, Mkami HE, Cammack R, Evans RW. 2007. Pulsed ELDOR determination of the intramolecular distance between the metal binding sites in Dicupric human serum transferrin and lactoferrin. *J. Am. Chem. Soc.* 129:4868–9.

63. Yang Z, Kise D, Saxena S. 2010. An Approach towards the Measurement of Nanometer Range Distances Based on Cu2+ Ions and ESR. *J. Phys. Chem. B.* 114:6165–6174.

64. Bode BE, Plackmeyer J, Prisner TF, Schiemann O. 2008. PELDOR measurements on a nitroxide-labeled Cu(II) porphyrin: orientation selection,

spin-density distribution, and conformational flexibility. *J. Phys. Chem. A.* 112:5064–73.

65. Raitsimring AM, Gunanathan C, Potapov A, Efremenko I, Martin JML *et al.* 2007. Gd3+ Complexes as Potential Spin Labels for High Field Pulsed EPR Distance Measurements. *J. Am. Chem. Soc.* 129:14138–14139.

66. Potapov A, Yagi H, Huber T, Jergic S, Dixon NE *et al.* 2010. Nanometer-scale distance measurements in proteins using Gd3+ spin labeling. *J. Am. Chem. Soc.* 132:9040–8.

67. Song Y, Meade TJ, Astashkin AV, Klein EL, Enemark JH, Raitsimring A. 2011. Pulsed dipolar spectroscopy distance measurements in biomacro-molecules labeled with Gd(III) markers. *J. Magn. Reson.* 210:59–68.

68. Narr E, Godt A, Jeschke G. 2002. Selective measurements of a nitroxide-nitroxide separation of 5 nm and a nitroxide-copper separation of 2.5 nm in a terpyridine-based copper(II) complex by pulse EPR spectroscopy. *Angew. Chem,. Int. Ed.* 41:3907–3910.

69. Lueders P, Jeschke G, Yulikov M. 2011. Double Electron-Electron Resonance Measured Between Gd3+ Ions and Nitroxide Radicals. *J. Phys. Chem. Lett.* 2:604–609.

70. Maryasov AG, Bowman MK, Tsvetkov YD. 2006. Dipole-dipole interactions of high-spin paramagnetic centers in disordered systems. *Appl. Magn. Reson.* 30:683–702.

71. Elsaesser C, Brecht M, Bittl R. 2002. Pulsed Electron-Electron Double Reso-nance on Multinuclear Metal Clusters: Assignment of Spin Projection Factors Based on the Dipolar Interaction. *J. Am. Chem. Soc.* 124:12606–12611.

72. Elsaesser C, Brecht M, Bittl R. 2005. Treatment of spin-coupled metal-

centres in pulsed electron-electron double-resonance experiments. *Biochem. Soc. Trans.* 33:15–9.

73. Milov AD, Naumov BD, Tsvetkov YD. 2004. The effect of microwave pulse duration on the distance distribution function between spin labels obtained by PELDOR data analysis. *Appl. Magn. Reson.* 26:587–599.

74. Banham JE, Baker CM, Ceola S, Day IJ, Grant GH *et al.* 2008. Distance measurements in the borderline region of applicability of CW EPR and DEER: a model study on a homologous series of spin-labelled peptides. *J. Magn. Reson.* 191:202–18.

75. Ward R, Bowman A, El-Mkami H, Owen-Hughes T, Norman DG. 2009. Long distance PELDOR measurements on the histone core particle. *J. Am. Chem. Soc.* 131:1348–9.

76. Grote M, Polyhach Y, Jeschke G, Steinhoff H, Schneider E, Bordignon E. 2009. Transmembrane Signaling in the Maltose ABC Transporter MalFGK2-E: Periplasmic MalF-P2 Loop Communicates Substrate Availability to the ATP-Bound MalK Dimer. *J. Biol. Chem.* 284:17521–17526.

77. Margraf D, Bode BE, Marko A, Schiemann O, Prisner TF. 2007. Conformational flexibility of nitroxide biradicals determined by X-band PELDOR experiments. *Mol. Phys.* 105:2153–2160.

78. Pornsuwan S, Schafmeister CE, Saxena S. 2008. Analysis of the dynamical flexibility of bis-peptide nanostructures. *J. Phys. Chem. C.* 112:1377–1384.

79. Milov AD, Tsvetkov YD, Formaggio F, Crisma M, Toniolo C, Raap J. 2000. Self-Assembling Properties of Membrane-Modifying Peptides Studied by PELDOR and CW-ESR Spectroscopies. *J. Am. Chem. Soc.* 122:3843–3848.

80. Hilger D, Jung H, Padan E, Wegener C, Vogel K *et al.* 2005. Assessing oligomerization of membrane proteins by four-pulse DEER: pH-dependent dimerization of NhaA Na+/H+ antiporter of E. coli. *Biophys. J.* 89:1328–1338.

81. Bode BE, Margraf D, Plackmeyer J, Duerner G, Prisner TF, Schiemann O. 2007. Counting the Monomers in Nanometer-Sized Oligomers by Pulsed Electron-Electron Double Resonance. *J. Am. Chem. Soc.* 129:6736–6745.

82. Denysenkov VP, Prisner TF, Stubbe J, Bennati M. 2006. High-field pulsed electron-electron double resonance spectroscopy to determine the orientation of the tyrosyl radicals in ribonucleotide reductase. *Proc. Natl. Acad. Sci U. S. A.* 103:13386–90.

83. Polyhach Y, Godt A, Bauer C, Jeschke G. 2007. Spin pair geometry revealed by high-field DEER in the presence of conformational distributions. *J. Magn. Reson.* 185:118–129.

84. Schiemann O, Cekan P, Margraf D, Prisner TF, Sigurdsson ST. 2009. Relative Orientation of Rigid Nitroxides by PELDOR: Beyond Distance Measurements in Nucleic Acids. *Angew. Chem,. Int. Ed.* 48:3292–3295, S3291/1-S3291/23.

85. Milikisyants S, Groenen EJJ, Huber M. 2008. Observer-selective double electron-electron-spin resonance, a pulse sequence to improve orientation selection. *J. Magn. Reson.* 192:275–279.

86. Jeschke G, Panek G, Godt A, Bender A, Paulsen H. 2004. Data analysis procedures for pulse ELDOR measurements of broad distance distributions. *Appl. Magn. Reson.* 26:223–244.

87. Bowman MK, Maryasov AG, Kim N, deRose VJ. 2004. Visualization of dis-

tance distribution from pulsed double electron-electron resonance data. *Appl. Magn. Reson.* 26:23–39.

88. Chiang Y, Borbat PP, Freed JH. 2005. The determination of pair distance distributions by pulsed ESR using Tikhonov regularization. *J. Magn. Reson.* 172:279–295.

89. Chiang Y, Borbat PP, Freed JH. 2005. Maximum entropy: A complement to Tikhonov regularization for determination of pair distance distributions by pulsed ESR. *J. Magn. Reson.* 177:184–196.

90. Jeschke G, Chechik V, Ionita P, Godt A, Zimmermann H *et al.* 2006. Deer-Analysis2006 - a comprehensive software package for analyzing pulsed EL-DOR data. *Appl. Magn. Reson.* 30:473–498.

91. Jeschke   G.   2011.   *DeerAnalysis*   ETH   Zürich. http://www.epr.ethz.ch/software/index.

92. Domingo Köhler S, Spitzbarth M, Diederichs K, Exner TE, Drescher M. 2011. A short note on the analysis of distance measurements by electron paramagnetic resonance. *J. Magn. Reson.* 208:167–170.

93. Savitsky A, Dubinskii AA, Flores M, Lubitz W, Mobius K. 2007. Orientation-resolving pulsed electron dipolar high-field EPR spectroscopy on disordered solids: I. Structure of spin-correlated radical pairs in bacterial photosynthetic reaction centers. *J. Phys. Chem. B.* 111:6245–62.

94. Lovett JE, Bowen AM, Timmel CR, Jones MW, Dilworth JR *et al.* 2009. Structural information from orientationally selective DEER spectroscopy. *Phys. Chem. Chem. Phys.* 11:6840–8.

95. Marko A, Margraf D, Cekan P, Sigurdsson ST, Schiemann O, Prisner TF. 2010. Analytical method to determine the orientation of rigid spin labels in

DNA. *Phys. Rev. E.* 81:021911.

96. Sale K, Song L, Liu Y, Perozo E, Fajer P. 2005. Explicit Treatment of Spin Labels in Modeling of Distance Constraints from Dipolar EPR and DEER. *J. Am. Chem. Soc.* 127:9334–9335.

97. Hilger D, Polyhach Y, Padan E, Jung H, Jeschke G. 2007. High-resolution structure of a Na+/H+ antiporter dimer obtained by pulsed electron paramagnetic resonance distance measurements. *Biophys. J.* 93:3675–3683.

98. Polyhach Y, Bordignon E, Jeschke G. 2011. Rotamer libraries of spin labelled cysteines for protein studies. *Phys. Chem. Chem. Phys.* 13:2356–2366.

99. Finiguerra MG, Prudencio M, Ubbink M, Huber M. 2008. Accurate long-range distance measurements in a doubly spin-labeled protein by a four-pulse, double electron-electron resonance method. *Magn. Reson. Chem.* 46:1096–101.

100. Banham JE, Jeschke G, Timmel CR. 2007. Evidence from EPR that nitroxide spin labels attached to human hemoglobin alter their conformation upon freezing. *Mol. Phys.* 105:2041–2047.

101. Lillington JE, Lovett JE, Johnson S, Roversi P, Timmel CR, Lea SM. 2010. Shigella flexneri Spa15 crystal structure verified in solution by double electron electron resonance. *J. Mol. Biol.* 405:427–35.

102. Appel M, Hizlan D, Vinothkumar KR, Ziegler C, Kuhlbrandt W. 2009. Conformations of NhaA, the Na/H exchanger from Escherichia coli, in the pH-activated and ion-translocating states. *J. Mol. Biol.* 386:351–65.

103. Galiano L, Blackburn ME, Veloro AM, Bonora M, Fanucci GE. 2009. Solute effects on spin labels at an aqueous-exposed site in the flap region of HIV-1 protease. *J. Phys. Chem. B.* 113:1673–80.

104. Fleissner MR, Cascio D, Hubbell WL. 2009. Structural origin of weakly ordered nitroxide motion in spin-labeled proteins. *Protein. Sci* 18:893–908.

105. Gruene T, Cho MK, Karyagina I, Kim HY, Grosse C *et al.* 2011. Integrated analysis of the conformation of a protein-linked spin label by crystallography, EPR and NMR spectroscopy. *J. Biomol. NMR.* 49:111–9.

106. Sali A, Blundell TL. 1993. Comparative protein modelling by satisfaction of spatial restraints. *J. Mol. Biol.* 234:779–815.

107. Brunger AT, Adams PD, Clore GM, DeLano WL, Gros P *et al.* 1998. Crystallography & NMR system: A new software suite for macromolecular structure determination. *Acta Crystallogr. D. Biol. Crystallogr.* 54:905–21.

108. Bhatnagar J, Freed JH, Crane BR. 2007. Rigid body refinement of protein complexes with long-range distance restraints from pulsed dipolar ESR. *Methods. Enzymol.* 423:117–133.

109. Borbat PP, Freed JH. 2007. Measuring distances by pulsed dipolar ESR spectroscopy: spin-labeled histidine kinases. *Methods. Enzymol.* 423:52–116.

110. Gordon-Grossman M, Gofman Y, Zimmermann H, Frydman V, Shai Y *et al.* 2009. A combined pulse EPR and Monte Carlo simulation study provides molecular insight on peptide-membrane interactions. *J. Phys. Chem. B.* 113:12687–95.

111. Hilger D, Polyhach Y, Jung H, Jeschke G. 2009. Backbone structure of transmembrane domain IX of the Na+/proline transporter PutP of Escherichia coli. *Biophys. J.* 96:217–225.

112. Jao CC, Hegde BG, Chen J, Haworth IS, Langen R. 2008. Structure of membrane-bound alpha-synuclein from site-directed spin labeling and computational refinement. *Proc. Natl. Acad. Sci U. S. A.* 105:19666–71.

113. Rao JN, Jao CC, Hegde BG, Langen R, Ulmer TS. 2010. A combinatorial NMR and EPR approach for evaluating the structural ensemble of partially folded proteins. *J. Am. Chem. Soc.* 132:8657–68.

114. Ward R, Zoltner M, Beer L, El MH, Henderson IR *et al.* 2009. The Orientation of a Tandem POTRA Domain Pair, of the Beta-Barrel Assembly Protein BamA, Determined by PELDOR Spectroscopy. *Structure (Cambridge, MA,. U. S).* 17:1187–1194.

115. Yang Y, Ramelot TA, McCarrick RM, Ni S, Feldmann EA *et al.* 2010. Combining NMR and EPR Methods for Homodimer Protein Structure Determination. *J. Am. Chem. Soc.* 132:11910–11913.

116. Leaver-Fay A, Tyka M, Lewis SM, Lange OF, Thompson J *et al.* 2010. ROSETTA3: an object-oriented software suite for the simulation and design of macromolecules. *Methods. Enzymol.* 487:545–74.

117. Lin M, Lu H, Chen R, Liang J. 2008. Generating properly weighted ensemble of conformations of proteins from sparse or indirect distance constraints. *J. Chem. Phys.* 129:094101/1–094101/13.

118. Hirst SJ, Alexander N, Mchaourab HS, Meiler J. 2011. RosettaEPR: An integrated tool for protein structure determination from sparse EPR data. *J. Struct. Biol.* 173:506–514.

119. Alexander N, Bortolus M, Al-Mestarihi A, Mchaourab H, Meiler J. 2008. De novo high-resolution protein structure determination from sparse spin-labeling EPR data. *Structure* 16:181–95.

120. Zheng W, Brooks BR. 2006. Modeling protein conformational changes by iterative fitting of distance constraints using reoriented normal modes. *Biophys. J.* 90:4327–36.

121. Polyhach Y, Jeschke G. 2010. Prediction of favourable sites for spin labelling of proteins. *Spectroscopy (Amsterdam, Neth)* 24:651–659.

122. Kazmier K, Alexander NS, Meiler J, Mchaourab HS. 2011. Algorithm for selection of optimized EPR distance restraints for de novo protein structure determination. *J. Struct. Biol.* 173:549–557.

123. Domingo Köhler S, Weber A, Howard SP, Welte W, Drescher M. 2010. The proline-rich domain of TonB possesses an extended polyproline II-like conformation of sufficient length to span the periplasm of Gram-negative bacteria. *Protein Sci.* 19:625–30.

124. Junk MJN, Spiess HW, Hinderberger D. 2010. The Distribution of Fatty Acids Reveals the Functional Structure of Human Serum Albumin. *Angew. Chem,. Int. Ed.* 49:8755–8759.

125. Akdogan Y, Junk MJN, Hinderberger D. 2011. Effect of Ionic Liquids on the Solution Structure of Human Serum Albumin. *Biomacromolecules* 12:1072–1079.

126. Altenbach C, Kusnetzow AK, Ernst OP, Hofmann KP, Hubbell WL. 2008. High-resolution distance mapping in rhodopsin reveals the pattern of helix movement due to activation. *Proc. Natl. Acad. Sci U. S. A.* 105:7439–7444.

127. Herget M, Baldauf C, Scholz C, Parcej D, Wiesmuller K *et al.* 2011. Conformation of peptides bound to the transporter associated with antigen processing (TAP). *Proc. Natl. Acad. Sci U. S. A.* 108:1349–1354, S1349/1-S1349/7.

128. Agafonov RV, Negrashov IV, Tkachev YV, Blakely SE, Titus MA *et al.* 2009. Structural dynamics of the myosin relay helix by time-resolved EPR and FRET. *Proc. Natl. Acad. Sci U. S. A.* 106:21625–30.

129. Vileno B, Chamoun J, Liang H, Brewer P, Haldeman BD *et al.* 2011. Broad

disorder and the allosteric mechanism of myosin II regulation by phosphorylation. *Proc. Natl. Acad. Sci U. S. A.* 108:8218–23.

130. Smirnova I, Kasho V, Choe JY, Altenbach C, Hubbell WL, Kaback HR. 2007. Sugar binding induces an outward facing conformation of LacY. *Proc. Natl. Acad. Sci U. S. A.* 104:16504–9.

131. Kim M, Xu Q, Murray D, Cafiso DS. 2007. Solutes alter the conformation of the ligand binding loops in outer membrane transporters. *Biochemistry* 47:670–9.

132. Meyer S, Bohme S, Kruger A, Steinhoff HJ, Klare JP, Wittinghofer A. 2009. Kissing G domains of MnmE monitored by X-ray crystallography and pulse electron paramagnetic resonance spectroscopy. *PLoS Biol.* 7:e1000212.

133. Bohme S, Meyer S, Kruger A, Steinhoff HJ, Wittinghofer A, Klare JP. 2010. Stabilization of G domain conformations in the tRNA-modifying MnmE-GidA complex observed with double electron electron resonance spectroscopy. *J. Biol. Chem.* 285:16991–7000.

134. Galiano L, Ding F, Veloro AM, Blackburn ME, Simmerling C, Fanucci GE. 2009. Drug Pressure Selected Mutations in HIV-1 Protease Alter Flap Conformations. *J. Am. Chem. Soc.* 131:430–431.

135. Upadhyay AK, Borbat PP, Wang J, Freed JH, Edmondson DE. 2008. Determination of the oligomeric states of human and rat monoamine oxidases in the outer mitochondrial membrane and octyl beta-D-glucopyranoside micelles using pulsed dipolar electron spin resonance spectroscopy. *Biochemistry* 47:1554–66.

136. Seyedsayamdost MR, Chan CT, Mugnaini V, Stubbe J, Bennati M. 2007. PELDOR spectroscopy with DOPA-beta2 and NH2Y-alpha2s: distance mea-

surements between residues involved in the radical propagation pathway of
E. coli ribonucleotide reductase. *J. Am. Chem. Soc.* 129:15748–9.

137. Gulla SV, Sharma G, Borbat P, Freed JH, Ghimire H *et al.* 2009. Molecular-
scale force measurement in a coiled-coil peptide dimer by electron spin reso-
nance. *J. Am. Chem. Soc.* 131:5374–5.

11   Acronyms and Definitions list

EPR electron paramagnetic resonance

SDSL site-directed spin labeling

transverse relaxation loss of phase coherence of electron spin magnetization
and thus loss of signal due to random magnetic field fluctuations

exchange coupling interaction between electron spins due to overlap of their
wavefunctions, decays exponentially with distance

form factor contribution to the DEER signal that is caused by spins that belong
to the same protein molecule or protein complex

CW EPR continuous-wave EPR, provides information on spin label mobility,
accessibility to water and oxygen, and to distances below 1.8 nm

orientation selection pulses excite only part of the spectrum corresponding to
only part of the molecular orientations in the magnetic field

nuclear modulation superposition of the DEER signal by weak oscillations at
nuclear Zeeman frequencies

MTSL methanethiosulfonate spin label

Tikhonov regularization direct transformation of the form factor to the dis-
tance distribution by striking a compromise between fit quality and smooth

distribution

MD molecular dynamics

rotamers conformations of spin label side chains that are distinguished only by variation in the dihedral angles

sparse constraints set of constraints on distances, angles, and/or dihedrals that in itself is too small to fully specify the structure

coarse-graining reducing the number of degrees of freedom by combining several atoms into one particle

rigid-body approximation assumption that a part of a protein or protein complex does not change internal structure during a structural transition

12 Annotated references

- (2) Introduced the cleanest way of separating dipole-dipole interaction from other interactions and relaxation.

- (5) Explained how four-pulse DEER works and thus set the stage for optimization of experimental protocols.

- (13) Demonstrated that distance distributions can be reliably obtained.

- (16) Introduced important concepts in obtaining spin label distance constraints and relating them to protein structure.

- (29) Demonstrated a huge gain in distance range by perdeuteration of the protein.

- (40) The best performing spectrometer for DEER at the time of writing.

- (81) Clarified potential and limitations in counting spins in molecules by DEER.

- (98) Introduced an affordable and easily accessible method for predicting spin label conformational distribution.

- (113) Demonstrated the use of DEER distance constraints to characterize partially disordered proteins.

- (130) Detected the functionally relevant structural transition in a transporter that was elusive to x-ray crystallography.
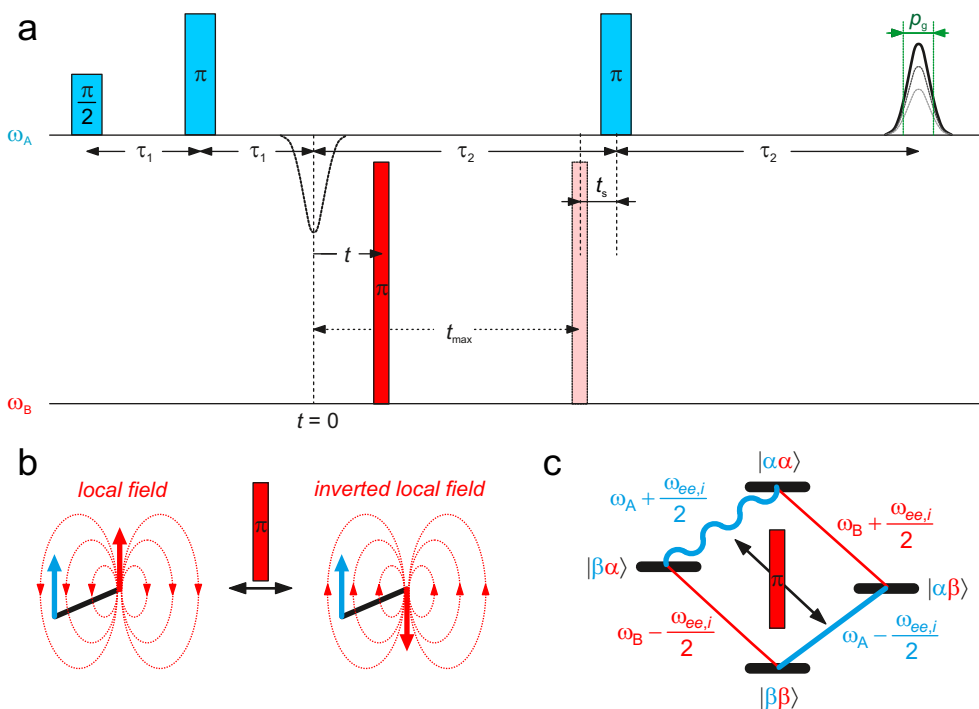
Figure 1: Four-pulse DEER experiment. (a) Pulse sequence. Time t is varied from $t < 0$ to t_{max} and variation of the integral echo intensity in the window of length p_{g} is recorded. (b) Local field picture. The π pump pulse at frequency ω_{B} inverts the state of spin B (red), thus inverting the local field imposed by spin B at the site of spin A (blue). (c) Energy level diagram. Inversion of the local field at spin A exchanges coherence between the two transitions of spin A that differ in frequency by $\omega_{ee,i}$.
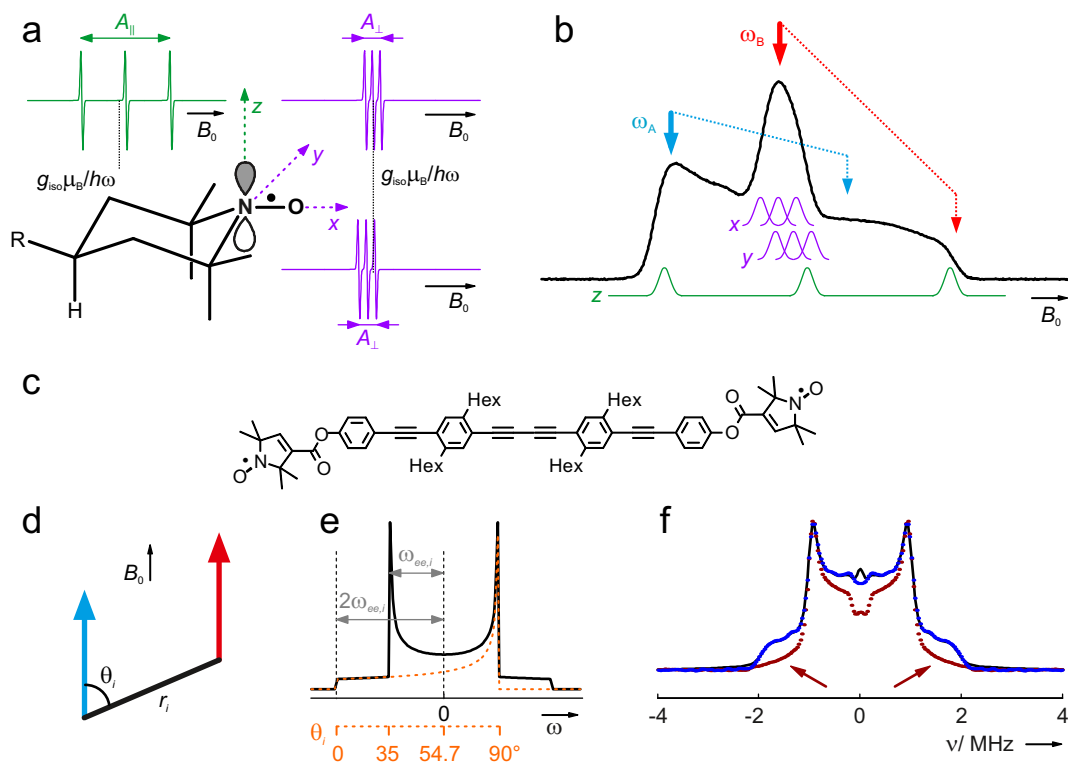
Figure 2: Orientation selection for nitroxide at X band. (*a*) Molecular frame and simulated continuous-wave (CW) EPR spectra along the principal axes. (*b*) Echo-detected EPR spectrum (black, superposition of absorption spectra of all orientations). At the standard pump position (red) all transitions in the xy plane and the center ^{14}N hyperfine component along z are excited. At the standard observer position (blue) mainly the low-field hyperfine component along z is excited. Orientation selection can be suppressed by variation of B_0, corresponding to a shift of observer and pump position along the blue and red dotted lines, respectively. (*c*) Structure of model compound **1**. (*d*) Distance vector between spin A (blue) and B (red) of length r_i at an angle θ_i with the magnetic field vector $\vec{B}_0$. (*e*) Dipolar spectrum (Pake pattern, solid line) as detected by DEER and correspondence of frequency $\omega_{ee,i}$ to angle θ_i (orange dotted line and scale). (*f*) Expected Pake pattern (black solid line), dipolar spectrum measured at standard pump and observer positions (maroon dotted line) and dipolar spectrum measured with orientation selection suppressed by a field scan (blue dotted line). Maroon arrows denote missing intensity corresponding to orientations with
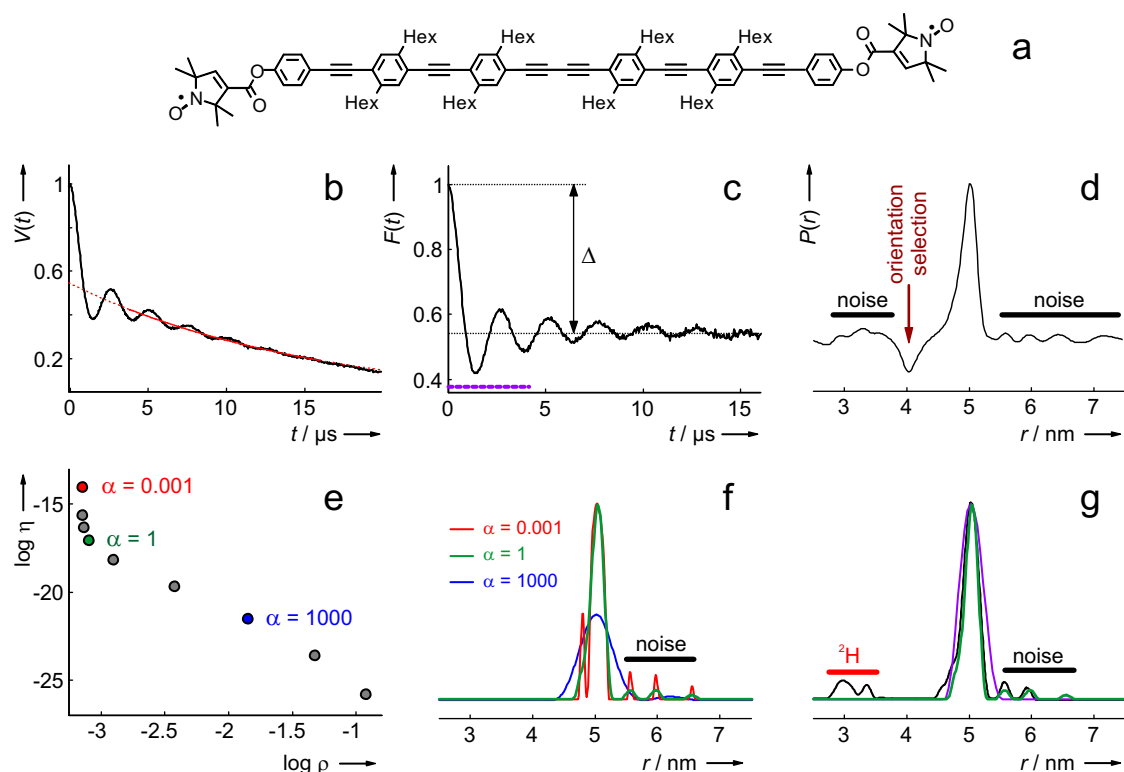
Figure 3: Data analysis and artifacts. (a) Structure of model compound **2**. (b) Primary four-pulse DEER data $V(t)$ of **2** (black line) and fitted background function $B(t)$ (red line). The dotted parts are extrapolated. (c) Form factor $F(t) = V(t)/B(t)$ with modulation depth Δ. The purple dashed line denotes the part accessible with $t_{max} = 4$ μs. (d) Distance distribution $P(r)$ obtained by approximate Pake transformation of $F(t)$. Black bars denote noise artifacts and the maroon arrow an orientation selection artifact (e) Tikhonov regularization L curve with three selected regularization parameters α. (f) Distance distributions obtained by Tikhonov regularization with constraint $P(r) > 0$. Undersmoothing (red) causes unrealistic peak splittings, oversmoothing (blue) causes artifical broadening, at the L curve corner (green), $P(r)$ is most realistic. (g) Best experimental distance distribution (green), artifacts due to missing nuclear modulation averaging (black line, red bar), and loss of shape when restricting data to $t_{max} = 4$ μs (purple).
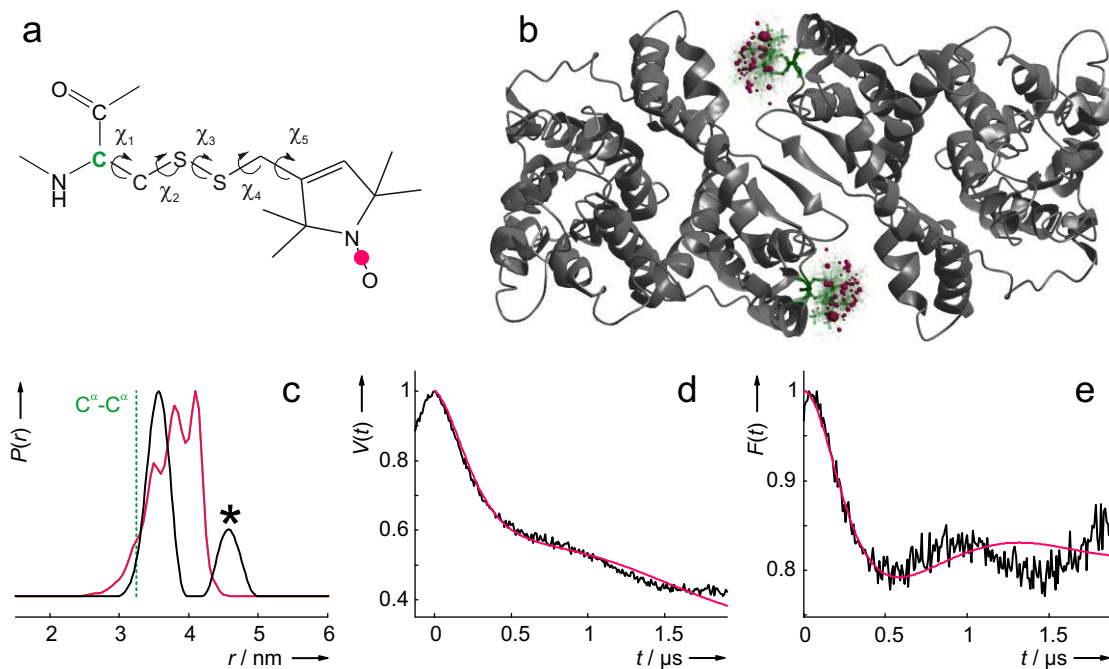
Figure 4: Spin label conformational distribution. (*a*) Five rotatable bonds (di-
hedrals $\chi_1 \ldots \chi_5$) cause distribution of the electron spin position (red dot) with
respect to the C^α atom (green). (*b*) Predicted conformational distribution of spin
labels at sites 202/202' of sodium/proton antiporter NhaA of *Escherichia coli*.
MTSL is shown by green stick models, red spheres visualize electron spin loca-
tion with their radii corresponding to rotamer populations. The prediction was
made by the rotamer library approach in MMM (47) and is based on the electron
microscopy model with PDB identifier 3FI1 (102). (*c*) Experimental (black) and
predicted (red) DEER distance distributions. The green dotted line denotes the
C^α-C^α distance. The asterisk denotes an aggregation artifact. (*d*) Best fit of
the primary DEER data (black) by the rotamer library prediction (red) obtained
by varying background decay rate $c_B K_B$ and modulation depth Δ. (*e*) Best fit
of the experimental form factor (black) by the prediction obtained by varying
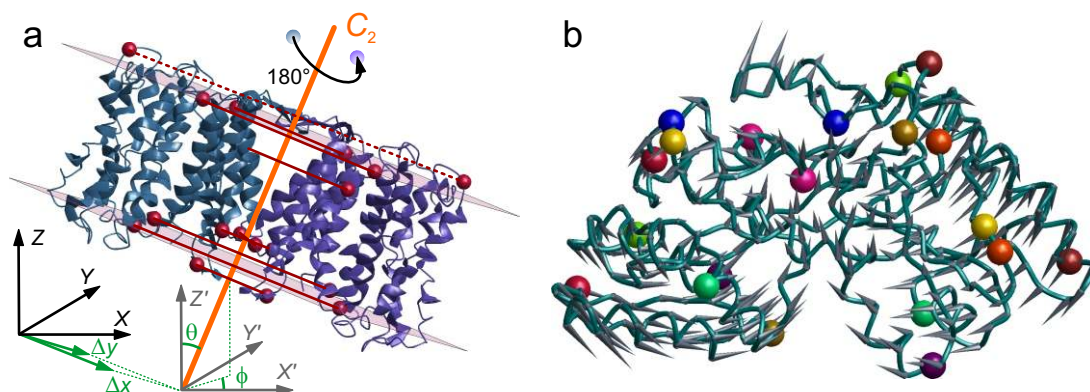modulation depth Δ.

Figure 5: Sparse distance constraints. (*a*) Determination of the relative arrangement of Na^+/H^+ antiporter monomers in a homodimer from nine distance constraints (red spheres denote labeling sites, red lines distance vectors) (97). Coordinates of the second monomer (violet) are obtained by rotation of coordinates of the first monomer (x-ray crystal structure 1ZCD, steelblue) bei 180° about the dimer C_2 axis (orange). Four free parameters (green) characterize orientation (polar angles θ and ϕ) of the C_2 axis in the crystal coordinate frame (black frame, capital letter axis identifiers) and translation of this axis (Δx and Δy) within the bilayer (semi-transparent pink planes). (*b*) Site pair selection by the Zheng/Brooks algorithm (120) for characterizing the structural transition of maltose binding protein MalE. The open apo structure (PDB 1OMP) is shown as a darkcyan string with grey cones denotig C^α atom motion on transition to the closed form (PDB 3MBP) in the presence of maltose. The ten suggested site pairs are indicated as pairs of C^α van-der-Waals spheres with matching colors. Distances range from 2.1 to 5.1 nm.